Werner syndrome helicase is a selective vulnerability of microsatellite instability-high tumor cells

Simone Lieb*[1], Silvia Blaha-Ostermann*[1], Elisabeth Kamper[1], Katharina Ehrenhöfer-Wölfer[1], Andreas Schlattl[1], Andreas Wernitznig[1], Jesse J. Lipp[1], Kota Nagasaka[2], Gerd Bader[1], Ralph A. Neumüller[1], Norbert Kraut[1], Mark A. Pearson[1], Mark Petronczki[1]*# and Simon Wöhrle[1]*#

[1]Boehringer Ingelheim RCV GmbH & Co KG, 1120 Vienna, Austria
[2]Research Institute of Molecular Pathology, Vienna Biocenter, 1030 Vienna, Austria

*Equal contribution
#Corresponding authors

mark_paul.petronczki@boehringer-ingelheim.com
simon.woehrle@boehringer-ingelheim.com

Running Title: WRN dependency in MSI-H cancer

Keywords: WRN, helicase, mismatch repair, microsatellite instability, colorectal cancer

Abstract

Targeted cancer therapy is based on exploiting selective dependencies of tumor cells. By leveraging recent large-scale genomic profiling and functional screening of cancer cell lines we identified Werner syndrome helicase (WRN) as a novel specific vulnerability of microsatellite instability-high (MSI-H) cancer cells. MSI, caused by defective mismatch repair is frequently detected in human malignancies, in particular in colorectal, endometrial and gastric cancers. We demonstrate that WRN inactivation selectively impairs the viability of MSI-H but not microsatellite stable (MSS) colorectal and endometrial cancer cell lines. In MSI-H cells, WRN loss results in the emergence of chromosome breaks, chromatin bridges and micronuclei highlighting defective genome integrity. WRN variants harboring mutations abrogating the ATPase function of WRN helicase fail to rescue the viability phenotype of WRN-depleted MSI-H colorectal cells. Our study suggests that pharmacological inhibition of WRN helicase function might represent a novel opportunity to develop a targeted therapy for MSI-H cancers.

Introduction

Defects in components of the DNA repair machinery, such as *BRCA1/2* mutations or impaired DNA mismatch repair (MMR), are a common characteristic of tumor cells, accelerating the accumulation of DNA mutations or chromosomal aberrations that are required for neoplastic transformation (Kinzler and Vogelstein 1997). Plasticity of genome stability pathways permits tumor cells to tolerate the loss of individual DNA repair genes and leads to synthetic lethality (SL) upon targeting the compensating repair mechanism (Nickoloff, Jones et al. 2017). The first clinically approved drugs exploiting such a SL interaction are Poly(ADP-Ribose) Polymerase (PARP) inhibitors for therapy of BRCA1/BRCA2-deficient tumors (Kaufman, Shapira-Frommer et al. 2015, Lord and Ashworth 2017).

MMR deficiency is caused by inactivation of genes of the DNA repair machinery involved in the resolution of nucleotide base-base mismatches during DNA replication (Jiricny 2006). MMR defects lead to characteristic variations in the length of tandem nucleotide repeats across the genome, known as microsatellite instability (MSI) (Aaltonen, Peltomaki et al. 1993, Ionov, Peinado et al. 1993, Peltomaki, Lothe et al. 1993). Germline mutations in MMR genes, most commonly MLH1, MSH2, MSH6 and PMS2, are causative for Lynch syndrome, a cancer predisposition condition associated with increased lifetime risk to develop colorectal cancer (CRC) or other tumor types including endometrial and gastric carcinoma (Lynch and Krush 1971, Mecklin and Jarvinen 1991, Hampel, Frankel et al. 2005). In sporadic, nonhereditary CRC, MSI is frequently observed due to epigenetic silencing of MLH1 (Cunningham, Christensen et al. 1998, Herman, Umar et al. 1998, Kuismanen, Holmberg et al. 2000). MSI-high (MSI-H) tumors display a hypermutator phenotype (Cancer Genome Atlas 2012), which entails increased immunogenicity, amendable to therapy with immune checkpoint inhibitors (Le, Uram et al. 2015). However, targeted therapies directly exploiting the MMR-deficient status of tumor cells do not exist.

Werner syndrome helicase (WRN) is a member of the RecQ DNA helicase subfamily (Yu, Oshima et al. 1996). RecQ helicases are involved in multiple DNA processing steps including DNA replication, double-strand break repair, transcription and telomere maintenance and are therefore considered to serve as “genome caretakers” (Chu and Hickson 2009). The critical function of this protein family in genome maintenance is underscored by the fact that defects in three of the five family members – WRN, Bloom Syndrome RecQ Like Helicase (BLM) and RecQ Like Helicase 4 (RECQL4) – give rise to human disease syndromes associated with developmental defects and cancer predisposition (Ellis, Groden et al. 1995, Yu, Oshima et al.

1996, Kitao, Shimamoto et al. 1999, Siitonen, Kopra et al. 2003, Van Maldergem, Siitonen et al. 2006). Specifically, patients with Werner syndrome display a premature ageing phenotype including arteriosclerosis, type II diabetes and osteoporosis and are prone to develop tumors of mesenchymal origin, such as soft tissue sarcoma or osteosarcoma (Hickson 2003, Goto, Ishikawa et al. 2013). WRN is unique among RecQ family helicases in possessing 3'-5' exonuclease activity (Huang, Li et al. 1998, Kamath-Loeb, Shen et al. 1998, Shen, Gray et al. 1998).

In contrast to the previously described tumor-suppressive role of WRN, we demonstrate in this study that WRN possesses a context-dependent critical pro-survival function for cancer cells. By leveraging a recently defined map of cancer cell specific vulnerabilities (McDonald, de Weck et al. 2017) and a comprehensive molecular characterization of cancer cell models (Barretina, Caponigro et al. 2012, Streit, Gratzl et al. 2018) we identify WRN helicase as a selective dependency in MSI-H cancer cell lines.

Results

WRN dependency is associated with MSI-H status of cancer cells

WRN was identified as a potential selective dependency in a subset of 398 cancer cell models in a recent pooled shRNA viability screen covering approximately 8000 genes (Project DRIVE) (McDonald, de Weck et al. 2017). A genomic or expression-based biomarker predictive for WRN dependency was unknown. Depletion of WRN exclusively affects viability of a subset of CRC, gastric and endometrial cancer cell models reflected by RSA (redundant siRNA activity) sensitivity scores ≤-3, indicative of cell essentiality (Figure 1A). Intriguingly, CRC, gastric and endometrial cancers are the three human malignancies with the highest frequency of MSI-H status (Cortes-Ciriano, Lee et al. 2017). This raised the possibility that WRN represents a selective dependency in MSI-H cell lines.

In order to explore this hypothesis we developed a Random Forest model using an MSI feature list defined by Boland and Goel (Boland and Goel 2010). This model classifies WRN sensitive and insensitive cell lines with an accuracy of 0.89 and a recall rate for sensitive lines of 0.69. Importantly, no true insensitive cell lines are classified as sensitive (Figure 1 – figure supplement 1A). An analysis of variable importance revealed MLH1 expression as the feature most highly associated with the classification outcome, in line with the frequent inactivation of the MLH1 gene in MSI-H CRC (Cunningham, Christensen et al. 1998, Herman, Umar et al. 1998, Kuismanen, Holmberg et al. 2000) (Figure 1 – figure supplement 1A). Consistently, WRN dependency anti-correlates with MLH1 mRNA expression levels among the cell models used in Project DRIVE (Figure 1 – figure supplement 1B; $p=1.02*10^{-4}$, stratification of MLH1-low and -high expressing cell models according to median MLH1 expression [TPM 37.44]).

Next, we wanted to experimentally validate the MSI status in a select set of cell lines. To this end, we used a fluorescent PCR-based analysis of five mononucleotide microsatellite markers to determine the MSS/MSI-H status of a subset of CRC, gastric and endometrial cancer cell models (Table 1). In addition, we utilized a comprehensive MSS/MSI-H status annotation of CRC cell models reported by Medico and colleagues (Medico, Russo et al. 2015). Analysis of gene dependency and MSS/MSI-H status data revealed that WRN dependency was strongly associated with MSI-H status across CRC, gastric and endometrial models ($p=6.11*10^{-8}$). Of the 19 cell lines classified as MSI-H, 15 cell lines (79%) were sensitive to WRN depletion using an RSA value of ≤-3 to define WRN dependency (Figure 1B). In contrast, WRN is dispensable for viability in all MSS cell models (Figure 1B). Our analysis suggests that MSI-H status is a strong predictor for WRN sensitivity of cancer cells.

WRN depletion by siRNA selectively impairs viability of MSI-H CRC and endometrial cancer cell lines

To experimentally corroborate the WRN dependency of MSI-H cancer cells, we applied short-interfering RNA (siRNA)-mediated knock-down of WRN in a panel of three MSS (SK-CO-1, CaCo-2, SW480) and three MSI-H (HCT 116, RKO, SNU-C4) CRC cell lines. In agreement with the results from Project DRIVE, WRN depletion using a mixture of four siRNA duplexes (Pool) or an individual siRNA (#1) targeting WRN profoundly affected viability in MSI-H, but not in MSS CRC models (Figure 2A). In contrast, depletion of the known essential mitotic kinase, PLK1, had a detrimental effect on viability of both MSS and MSI-H cell lines. Efficient depletion of WRN protein following siRNA transfection was confirmed by immunoblotting (Figure 2A). The selective dependency on WRN was mirrored in colony formation assays with two MSS (LS1034, SK-CO-1) and two MSI-H cell lines (HCT 116, RKO) (Figure 2B). Likewise, we observed that WRN knock-down impaired viability of three MSI-H endometrial carcinoma cells lines (HEC-265, ISHIKAWA, HEC-6), but not the MSS cell line MFE-280 (Figure 2C). WRN mRNA levels were similarly reduced upon transfection of pooled or individual WRN-targeting siRNAs in all four endometrial carcinoma models (Figure 2 – figure supplement 1A).

Similar to MSS cancer models, non-transformed telomerase-immortalized human retinal pigment epithelial cells (hTERT RPE-1) did not display sensitivity to knock-down of WRN. It is noteworthy, that the depletion of the related RecQ helicase BLM significantly impaired viability of hTERT RPE-1, but not HCT 116 cells (Figure 2 – figure supplement 1B). To assess a potential mechanism to bypass WRN dependence in MSI-H cancer cells, we tested whether co-depletion of p53 and WRN in the *TP53*-wild-type MSI-H CRC line HCT 116 would reverse the sensitivity to WRN knock-down. However, WRN/p53 co-depletion exacerbated the reduction in viability compared to WRN knock-down alone (Figure 2 – figure supplement 1C). *TP53*-wild-type MSS CRC SK-CO-1 cells were affected neither by individual or dual knock-down of WRN and p53. Interestingly, in both cell lines we observed a slight elevation of p53 protein levels upon WRN depletion (Figure 2 – figure supplement 1C). These RNAi experiments demonstrate that depletion of WRN abrogates viability in MSI-H but not MSS or non-transformed cells.

CRISPR/Cas9-mediated knock-out of WRN confirms the selective dependency of MSI-H CRC models on WRN

We carried out CRISPR-Cas9 depletion assays in MSS and MSI-H CRC models to independently confirm the selective WRN dependencies observed in shRNA/siRNA studies. Cell lines were stably transduced with Cas9 followed by transduction of lentiviral particles co-

expressing GFP and single guide RNAs (sgRNAs) targeting WRN or the essential replication factor RPA3 (Figure 3A). To investigate the relevance of the different protein domains in WRN by CRISPR scanning (Shi, Wang et al. 2015), domain specific sgRNAs were used to target the exonuclease, helicase, RecQ helicase family DNA-binding (RQC) and Helicase and RNase D C-terminal (HRDC) domains and the C-terminal helix-turn-helix (HTH) motif. Negative selection of sgRNA expressing cells was monitored over 14 days via flow cytometry-based quantification of GFP expressing cells, and normalized to the effect of the RPA3 positive control sgRNA (Figure 3B). We did not observe depletion of cells harboring WRN targeting sgRNAs in the MSS CRC cell line HT-29. In contrast, MSI-H HCT 116 cells expressing WRN sgRNAs depleted to a similar level as observed for the RPA3 positive control. SgRNA directed against the exonuclease, helicase and RQC domains were most effective, implying a functional or structural requirement of both these domains in the context of WRN dependency. Interestingly, strong depletion effects were also observed for sgRNAs targeting the C-terminal HTH motif (Figure 3B). A similar WRN sgRNA depletion pattern was observed in the MSI-H CRC cell line RKO, while we found far less pronounced depletion effects in the MSS CRC model SK-CO-1 (Figure 3 – figure supplement 1). In agreement with the RNAi studies, our CRISPR/Cas9 experiments suggest that WRN provides an essential gene function in two MSI-H CRC cell lines but not in two MSS CRC lines.

WRN dependency in MSI-H CRC is linked to its helicase function

To further dissect the relevance of WRN exonuclease and helicase function in WRN-dependent cell models, we generated FLAG-tagged, siRNA-resistant WRN (WRNr) expression constructs harboring loss-of-function mutations within the exonuclease- (E84A, Nuclease-dead) and helicase-domain (K577M, ATPase-dead), or both domains (E84A/K577M, Double-mutant) (Gray, Shen et al. 1997, Huang, Li et al. 1998) (Figure 4A). Wild-type and mutant forms of WRNr were transduced in HCT 116 cells and monoclonal lines with matched stable WRNr expression were generated. Expression and nuclear accumulation of transgenic WRNr variants among the cell lines was confirmed using immunofluorescence analysis (Figure 4B). Immunoblotting revealed that transgenic WRNr wild-type as well as the mutant WRN proteins were expressed at levels higher than the endogenous WRN counterpart (Figure 4B). Two wild-type WRNr expressing clones were selected based on the respective high and low expression of the transgene in order to cover the range of mutant WRNr variant expression observed in the selected panel of clones. As expected, viability of empty vector control-transduced cells was strongly reduced upon depletion of WRN (Figure 4C). Importantly, both the high and low expression level of wild-type WRNr was sufficient to render HCT 116 cells inert to knock-down of endogenous WRN (Figure 4C). This demonstrates the on-target effect of the WRN siRNA duplex and indicates that the

transgene-mediated rescue of WRN function is not protein level sensitive. Exogenous expression of the nuclease-dead form of WRNr almost completely rescued the effect of endogenous WRN depletion. In stark contrast, although expressed at similar or higher levels than WRNr wild-type, both the ATPase-dead and double-mutant form of WRNr were unable to restore viability following depletion of endogenous WRN (Figure 4C). Similarly, in RKO cells expressing WRNr variants, we also observed a stronger dependency on WRN helicase function compared to exonuclease activity upon knock-down of endogenous WRN (Figure 4 – figure supplement 1). These results indicate that the ATPase activity of WRN and possibly its helicase function are crucial for the survival of MSI-H CRC cells.

Loss of WRN causes mitotic defects and nuclear abnormalities in MSI-H cells

In order to investigate the cellular basis for the viability reduction of MSI-H cancer cells upon WRN depletion, we monitored the consequences of WRN loss-of-function using immunofluorescence analysis of the nuclear membrane protein LAP2β and Hoechst DNA staining in MSS and MSI-H CRC cell lines. SW480 did not display any phenotypic differences upon transfection with NTC and WRN-targeting siRNAs (Figure 5A). Strikingly, in HCT 116 and RKO cells we observed formation of chromatin bridges and micronuclei upon WRN knock-down, both potential consequences of failed sister genome partitioning during mitosis (Figure 5A). Enlarged nuclei, indicative of failed mitosis, were additionally observed upon WRN knock-down in HCT 116 cells. Quantification of the frequency of chromatin bridges and micronuclei revealed that WRN depletion did not affect baseline levels of these aberrant nuclear morphologies in the MSS CRC cancer models SK-CO-1 and SW480, while the frequency of both chromatin bridges and micronuclei was strongly increased upon WRN knock-down in the MSI-H CRC cell lines HCT 116 and RKO (Figures 5B and C). In non-transformed hTERT RPE-1 cells, WRN depletion led to a slight increase of chromatin bridge and micronucleus formation, although far less pronounced compared to the MSI-H CRC models (Figures 5B and C). Supportive of the immunofluorescence studies, live cell imaging revealed a strong increase of the incidence of lagging chromosomes and chromosome bridges during mitosis in WRN depleted MSI-H CRC cell lines HCT 116 and RKO, but not MSS SW480 cells (Figure 6). We conclude that WRN depletion in MSI-H cells results in nuclear morphology and integrity aberrations that are manifested during cell division. The correlation of these defects with the observed cell viability reduction in MSI-H models suggests that nuclear abnormalities are causally linked to the anti-proliferative effect of WRN loss.

Structural chromosome aberrations in MSI-H cells after WRN loss-of-function

The observed nuclear integrity and mitotic defects caused by WRN depletion in MSI-H cells could be the consequence of preceding genome maintenance aberrations. This hypothesis is reinforced by the important role of RECQ family helicases, including WRN, in genome integrity (Chu and Hickson 2009). To interrogate genome integrity, we performed mitotic chromosome spread analysis in MSI-H, MSS and non-transformed cells after depletion of WRN. To overcome the low abundance of mitotic cells in WRN-depleted MSI-H cell lines, caffeine was added to cultured cells to bypass the G2/M checkpoint. Strikingly, WRN loss elicited structural chromosome aberrations, such as chromosome breaks and non-homologous radial formations, in the MSI-H CRC cell lines HCT 116 and RKO (Figure 7A). Quantification of the number of chromatin breaks per nuclei demonstrated a strong increase in the fraction of cells harboring 1-5 or >5 chromosome breaks per nuclei in the two MSI-H CRC models upon WRN depletion (Figure 7B). In the MSS CRC model SW480 and hTERT RPE1 non-transformed cells only a minor increase of nuclei with chromosome breaks was detected (Figure 7B). These data suggest that WRN helicase is essential for maintaining genome integrity in MSI-H cells by preventing chromosome breaks and erroneous chromosome fusions. The observed mitotic chromosome aberrations in WRN-depleted MSI cells can also explain the aforementioned nuclear morphology and mitotic defects, including micronuclei, lagging chromosomes and chromatin bridges. The correlation of chromosome aberrations and nuclear abnormalities with MSI-H status following loss of WRN function suggests that genome integrity defects are responsible for the profound reduction in viability of MSI-H cancer cells.

Discussion

Treatment paradigms for MSI-H tumors have recently shifted with the approval of the immune checkpoint agents pembrolizumab, nivolumab and ipilimumab, targeting programmed cell death 1 (PD-1) and cytotoxic T-lymphocyte-associated Protein 4 (CTLA-4) in this patient segment (Le, Uram et al. 2015, Le, Durham et al. 2017, Overman, Lonardi et al. 2018). Pembrolizumab constitutes the first cancer therapy approval based on a patient selection biomarker irrespective of the tumor type, highlighting MSI-H status as a therapeutically trackable and clinically implemented feature of tumor cells (Goswami and Sharma 2017). While responses to immune checkpoint blockade in MSI-H cancer are often durable, intrinsic and acquired resistance to immunotherapy represents a continuous medical need in MSI-H cancer.

The results of this study uncover a novel vulnerability of MSI-H tumor cell models and indicate that pharmacological inhibition of WRN ATPase/helicase function might serve as an attractive novel targeted therapeutic strategy in MSI-H cancer. Our data suggest that similar to the tumor agnostic activity of checkpoint blockade, MMR deficiency represents a genetic determinant for WRN dependency regardless of tumor type. Upon WRN loss-of-function we observe a strong and rapid decrease in viability of MSI-H cell models that is accompanied by nuclear abnormalities and cell division defects. In particular, we find that WRN depleted MSI-H cancer cells display chromosome breaks, chromatin bridges and micronuclei indicative of genome instability that is highlighted during cell division. The occurrence of these defects in MSI-H but not MSS cells upon WRN inactivation suggests that these aberrations might be causally linked to the selective reduction in viability in MSI-H cells. While rescue studies using WRN variants clearly indicate WRN helicase function as the critical enzymatic activity in MSI-H cell models, CRISPR domain scanning suggests a structural requirement of the exonuclease domain and the HTH loop of WRN.

WRN is a member of the RecQ helicase family which fulfils pleiotropic functions in DNA repair (Chu and Hickson 2009). MMR activity is required for activation of the G2/M checkpoint in response to DNA damage prior to entry into mitosis (O'Brien and Brown 2006). WRN function in MSI-H cells might therefore be critical for the resolution of DNA damage events and to prevent premature entry into mitosis. Of note, cell lines derived from Werner syndrome patients display defective mitotic recombination and are susceptible to genome instability (Prince, Emond et al. 2001). However, in MSS cancer and non-transformed cells WRN depletion had no or very mild effects on viability, suggesting that pharmacological inhibition of WRN might allow for an MSI-H cancer-directed therapy that spares normal cells and tissues.

The chromosome breaks and radial chromosomes observed in MSI-H cells upon WRN depletion indicate the generation and/or persistence of DNA double strand breaks. Future research is required to dissect the molecular basis for this effect. It is conceivable that WRN is required to process and resolve DNA repair or replication intermediates that arise in MMR-deficient cells or that MMR is required to cope with intermediates emerging upon compromised WRN function. The identification of the molecular basis of the WRN-MSI-H relationship will also help to understand why some rare outlier MSI-H cell lines do not respond to WRN inactivation.

Werner syndrome patients show an increased lifetime risk to develop tumors, pointing to a tumor-suppressive function of WRN (Goto, Ishikawa et al. 2013). Interestingly, homozygous *Wrn*-null mice display no overt phenotype and do not recapitulate the premature ageing or cancer predisposition conditions of Werner syndrome, unless crossed into a *Terc*-null background (Lebel and Leder 1998, Lombard, Beard et al. 2000, Chang, Multani et al. 2004). Mutations in Werner syndrome are almost exclusively truncating nonsense, splicing or frameshift mutations affecting WRN nuclear localization, suggesting that concomitant loss of WRN helicase and exonuclease function might be required for the onset of Werner syndrome (Matsumoto, Shimamoto et al. 1997, Huang, Lee et al. 2006). This indicates that inhibition of WRN helicase function might have a therapeutic index for the treatment of MSI-H cancer without inducing Werner syndrome related phenotypes.

Our study highlights the power of combining deep functional genomic screen data with tumor cell line profiling to identify new targets with an associated predictive biomarker in oncology. Given the possibility to develop potent and selective small molecule inhibitors of WRN helicase (Rosenthal, Dexheimer et al. 2010), our findings outline a novel strategy for the treatment of a clinically defined subset of patients harboring MSI-H/MMR-deficient tumors. Since genome instability can elicit cytoplasmic nucleic acid sensor pathways and innate immune responses (Mackenzie, Carroll et al. 2017), the induction of cancer cell selective nuclear aberrations by WRN inactivation could provide a synergistic combination option with the approved immunotherapy agents for the benefit of MSI-H cancer patients.

Materials and Methods

Random Forrest model

To explore the hypothesis that WRN sensitivity is associated with MSI, we employed an exploratory machine learning approach (Qi 2012). We first divided the DRIVE WRN cell line sensitivity data (McDonald, de Weck et al. 2017) into four distinct groups, using a k-means clustering algorithm. We chose four clusters to model insensitive (cluster 1), moderate insensitive (cluster 2), moderate sensitive (cluster 3) and sensitive (cluster 4) cell lines. We subsequently denoted clusters 1 and 2 as insensitive and clusters 3 and 4 as sensitive and chose an RSA score < -1.37 (maximum value of cluster 3) as a cutoff between sensitive and insensitive lines. Only a small fraction of cell lines, 30 out of 371 cell lines (8%), is sensitive in the entire data set, suggesting a pronounced class imbalance between sensitive and insensitive cell lines. To address this class imbalance, we focused our subsequent analysis on cell lines originating from CRC, as i) most sensitive cell lines are from this indication and ii) MSI has been extensively characterized in this indication (Boland and Goel 2010, Medico, Russo et al. 2015). 36% (13 out of 36) of colon cancer cell lines are sensitive to WRN loss of function according to our k-means clustering based approach.

We next assembled a MSI feature list. We used cell line gene expression and mutation data for the cell lines from a set of genes, i) involved in MMR (EXO1, MLH1, MLH3, MSH2, MSH3, MSH6) and ii) genetic target genes of MSI in CRC (Boland and Goel 2010). We next trained a Random Forest model based on 50% of the data. On the full dataset, the model classifies WRN sensitive and insensitive cell lines with an accuracy of 0.89 and a recall rate for sensitive lines of 0.69.

MSI Analysis

Genomic DNA was isolated using QIAamp®DNA mini kit (Qiagen, Hilden, Germany). Per reaction 2 ng of genomic DNA was used for fluorescent PCR-based analysis of the mononucleotide microsatellite marker length using the Promega MSI Analysis System, Version 1.2 kit. Microsatellite fragment length was analyzed using capillary electrophoreses (Applied Biosystems 3130xl Genetic Analyzer, 16-capillary electrophoresis instrument) and evaluated with GeneMapper Software 5 (Applied Biosystems).

Cell culture and lentiviral transduction

HCT 116 cells were cultured in McCoy's 5A medium (GIBCO, 36600-021) with glutamax supplemented with 10% fetal calf serum (FCS), hTERT RPE-1 cells were cultured in DMEM:F12

(ATCC: 30–2006) supplemented with 10% FCS and 0.01 mg/ml Hygromycin B. RKO, SW480, CaCo-2 and SK-CO-1 cells were cultured in EMEM (SIGMA, M5650) with glutamax supplemented with 10% FCS and Na-Pyruvate. SNU-C4 cells were cultured in RPMI1640 medium (ATCC #30-2001) with glutamax, supplemented with 10% FCS, 25 mM HEPES and 25 mM NaHCO3. LS1034 cells were cultured in RPMI-1640 (ATCC #30-2001) supplemented with 10% FCS. MFE-280 cells were cultured in 40% RPMI 1640 (GIBCO), 40% DMEM (SIGMA, D6429) supplemented with 20% FCS and 1X insulin-transferin-sodium selenite (GIBCO, 41400-045). HEC-265 cells were cultured in EMEM (SIGMA, M5650) with glutamax supplemented with 15% FCS. ISHIKAWA cells were cultured in EMEM (SIGMA, M5650) w/glutamax medium supplemented with 5% FCS and NEAA. HEC-6 cells were cultured in EMEM (SIGMA, M5650) with glutamax supplemented with 15% FCS and NEAA and Na-Pyruvate. HT-29_CRISPR-Cas9 cells were cultured in McCoy's 5A (GIBCO, 36600-021) with glutamax supplemented with 10% FCS and 10 µg/ml Blasticidin (Invitrogen, R210-01). HCT 116 _CRISPR-Cas9 cells were cultured like the parental cell line supplemented with 2 µg/ml Puromycin. All supplements were obtained from GIBCO, FCS (SH30071.03) from GE Healthcare Life Sciences and Puromycin from SIGMA (P9620). Lentiviral particles were produced using the Lenti-X Single Shot system (Clontech, Mountain View, CA, US). Following lentiviral infection, stably transduced pools were generated using Puromycin selection (HCT 116: 2 µg/ml, RKO: 0.5 µg/ml, SK-CO-1: 1 µg/ml) or Blasticidin (HT-29: 10 µg/ml). Sources, MSI status and authentication information (STR fingerprinting at Eurofins Genomics, Germany) of cell lines used in this study are provided in Table 2. All cell lines were tested negatively for mycoplasma contamination and have been authenticated by STR fingerprinting.

siRNA transfection and cell viability

For knock-down experiments, cells were transfected with ON-TARGETplus SMARTpool siRNA duplexes (Dharmacon, Lafayette, CO, US) using Lipofectamine RNAiMAX reagent according to the manufacturer's instructions (Invitrogen, Waltham, MA, US). For WRN knock-down, additionally an individual siRNA was used (J-010378-05). Chromosome spreads, immunoblotting, immunofluorescence and live cell imaging experiments were performed using a final siRNA concentration of 20 nM. Cell viability and crystal violet staining assays were performed using 10 nM siRNA. Viability was determined using CellTiter-Glo (Promega, Madison, WI, US) and by staining with crystal violet (Sigma-Aldrich, St. Louis, MO, US; HT901). For co-depletion of p53 and WRN 10 nM of the respective siRNA duplexes each were used for immunoblot and viability assay.

372 **Cell extracts for immunoblotting**

373 Cell pellets were resuspended in extraction buffer (50 mM Tris Cl pH 8.0, 150 mM NaCl, 1%
374 Nonidet P-40 supplemented with Complete protease inhibitor mix (Roche, Switzerland) and
375 Phosphatase inhibitor cocktails (Sigma-Aldrich, St. Louis, MO, US; P5726 and P0044).

376 **Antibodies**

377 The following antibodies were used: WRN (8H3) mouse mAb (Cell signaling #4666, 1/1000
378 dilution), mouse anti-GAPDH (Abcam, ab8245, 1/30000 dilution), mouse anti-FLAG (SIGMA,
379 F1804, 1/1000 [immunoblot] or 1/500 [immunofluorescence] dilution), mouse anti-LAP2ß (BD
380 (Transduction Laboratories #611000, 1/100 dilution), mouse anti-p53 (Calbiochem, OP43,
381 1/1000 dilution) and secondary rabbit (Dako P0448, 1/1000 dilution), mouse anti-IgG-HRP(Dako
382 P0161, 1/1000 dilution) and mouse Alexa Fluor 488 (Molecular Probes, Eugene, OR, US,
383 1/1000 dilution).

384 **Quantitative reverse transcription PCR (qRT-PCR)**

385 RNA was isolated 72 h post-transfection and reversely transcribed using SuperScript™ VILO™
386 kit (Thermo Scientific). All qPCR analyses were performed with the QuantiTect® Multiplex PCR
387 kit (Qiagen, Hilden, Germany) on a StepOne Real-Time PCR Sytem™ (Applied Biosytems) with
388 a total of 45 cycles. Constitutive maintenance gene 18S rRNA (Applied Biosystems, Quencher
389 VIC®/MGB, 4319413E) and human WRN (Applied Biosystems, Quencher FAM®/MGB-NFQ,
390 4331182) TaqMan probes were used. WRN expression was normalized to 18S rRNA expression
391 levels and is indicated relative to the NTC control.

392 **CRISPR depletion assays**

393 Stable Cas9 expressing cell lines, using either Blasticidin or Puromycin as selection markers,
394 were transduced with vectors encoding GFP and sgRNAs targeting different domains of WRN
395 (Table 3). On day 3 post-transfection the fraction of GFP positive cells, measured via flow
396 cytometry analysis, was set to 100%. All values were normalized to the control RPA3_1.3 for
397 relative depletion ratio.

398 **cDNA transgene vectors**

399 pLVX-WRN-3xFLAG-IRES-Puro, pLVX-WRN-3xFLAG-IRES-Puro K577M, pLVX-WRN-3xFLAG-
400 IRES-Puro E84A and pLVX-WRN-3xFLAG-IRES-Puro E84A _K577M for siRNA-resistant
401 transgene expression were generated by gene synthesis (GenScript, China) based on the WRN
402 cDNA sequence NCBI NM_000553.5 followed by cloning into the parental pLVX vector

(Clontech, Mountain View, CA, US). Codon optimization changes were introduced into WRN coding sequences to render the transgenes siRNA-resistant.

Immunofluorescence, **chromosome spreads and live cell imaging**

For immunofluorescence, 72 h post siRNA transfection cells were fixed with 4% paraformaldehyde for 15 min, permeabilized with 0.2% Triton X-100 in PBS for 10 min and blocked with 3% BSA in PBS containing 0.01% Triton X-100. Cells were incubated with primary (LAP2ß) and secondary antibody (Alexa 488, Molecular Probes, Eugene, OR, US), DNA was counterstained with Hoechst 33342 (Molecular Probes, Eugene, OR, US; H3570). Coverslips and chambers were mounted with ProLong Gold (Molecular Probes, Eugene, OR, US). Images were taken with an Axio Plan2/AxioCam microscope and processed with MrC5/Axiovision software (Zeiss, Germany). For chromosome spread analysis, Nocodazole (1.5 µM final concentration) and 2 mM Caffeine was added to the medium for 6 h. Cells were harvested and hypotonically swollen in 40% medium/60% tap water for 5 min at room temperature. Cells were fixed with freshly made Carnoy's solution (75% methanol, 25% acetic acid), and the fixative was changed three times. For spreading, cells in Carnoy's solution were dropped onto glass slides and dried. Slides were stained with 5% Giemsa (Merck) for 4 min, washed briefly in tap water and air dried. For chromosome spread analysis two independent slides were scored blindly for each condition. Live cell imaging was performed using Spinning Disk Confocal UltraView Vox Axio Observer equipped with Plan apochromat 20x/0.8 objective (Zeiss) and an electron-multiplying charge-coupled device 9100-13 camera (Hamamatsu Photonics). The microscope was controlled using Volocity software (Perkin-Elmer). DNA was counterstained with 100 nM SiR-Hoechst 3 h before the start of imaging. At 24 h post siRNA transfection cell nuclei were imaged in 2 z slice sections spaced 6 µm every 6 min for 48 h. For the imaging, cells were seeded into glass bottom 24 well SensoPlate (Greiner) with imaging medium (phenol red free DMEM supplemented with 10% [vol/vol] FCS, L-glutamine 2 mM and 1% [vol/vol] penicillin-streptomycin). During live cell imaging, cells were maintained at 37°C in a humidified 5% CO_2 atmosphere.

Acknowledgements

We would like to thank Susanne Stockinger, Vanessa Rössler, Jodie Grant und Christoph Reiser (all Boehringer Ingelheim RCV GmbH) for generation of Cas9-expressing cell lines. The Research Institute of Molecular Pathology (IMP) is supported by Boehringer Ingelheim. We thank Stephen West (The Francis Crick Institute, UK) for helpful suggestions and advice. We are grateful to Jan-Michael Peters (IMP) for support of this study and access to live cell imaging technology. KN is supported by an EMBO Long Term Fellowship (ALTF 1335-2016) and a HFSP fellowship (LT001527/2017).

Author contributions

SL, SBO, EK, KEW and KN performed the experiments. GB designed exonuclease- and ATPase-dead WRN expression constructs. AS, AW, JJL and RAN performed bioinformatic analyses. MAP and NK supervised the study. MP and SW wrote the manuscript with support from SL, SBO, EK and RAN. MP and SW designed and supervised the experiments and devised the main conceptual ideas.

Conflict of interest

SL, SBO, EK, KEW, AS, AW, JJL, GB, RAN, NK, MAP, MP and SW are full-time employees of Boehringer Ingelheim RCV GmbH & Co KG, Vienna, Austria. KN declares that no competing interests exist.

References

Aaltonen, L. A., P. Peltomaki, F. S. Leach, P. Sistonen, L. Pylkkanen, J. P. Mecklin, H. Jarvinen, S. M. Powell, J. Jen, S. R. Hamilton and et al. (1993). "Clues to the pathogenesis of familial colorectal cancer." Science **260**(5109): 812-816.

Barretina, J., G. Caponigro, N. Stransky, K. Venkatesan, A. A. Margolin, S. Kim, C. J. Wilson, J. Lehar, G. V. Kryukov, D. Sonkin, A. Reddy, M. Liu, L. Murray, M. F. Berger, J. E. Monahan, P. Morais, J. Meltzer, A. Korejwa, J. Jane-Valbuena, F. A. Mapa, J. Thibault, E. Bric-Furlong, P. Raman, A. Shipway, I. H. Engels, J. Cheng, G. K. Yu, J. Yu, P. Aspesi, Jr., M. de Silva, K. Jagtap, M. D. Jones, L. Wang, C. Hatton, E. Palescandolo, S. Gupta, S. Mahan, C. Sougnez, R. C. Onofrio, T. Liefeld, L. MacConaill, W. Winckler, M. Reich, N. Li, J. P. Mesirov, S. B. Gabriel, G. Getz, K. Ardlie, V. Chan, V. E. Myer, B. L. Weber, J. Porter, M. Warmuth, P. Finan, J. L. Harris, M. Meyerson, T. R. Golub, M. P. Morrissey, W. R. Sellers, R. Schlegel and L. A. Garraway (2012). "The Cancer Cell Line Encyclopedia enables predictive modelling of anticancer drug sensitivity." Nature **483**(7391): 603-607.

Boland, C. R. and A. Goel (2010). "Microsatellite instability in colorectal cancer." Gastroenterology **138**(6): 2073-2087 e2073.

Cancer Genome Atlas, N. (2012). "Comprehensive molecular characterization of human colon and rectal cancer." Nature **487**(7407): 330-337.

Chang, S., A. S. Multani, N. G. Cabrera, M. L. Naylor, P. Laud, D. Lombard, S. Pathak, L. Guarente and R. A. DePinho (2004). "Essential role of limiting telomeres in the pathogenesis of Werner syndrome." Nat Genet **36**(8): 877-882.

Chu, W. K. and I. D. Hickson (2009). "RecQ helicases: multifunctional genome caretakers." Nat Rev Cancer **9**(9): 644-654.

Cortes-Ciriano, I., S. Lee, W. Y. Park, T. M. Kim and P. J. Park (2017). "A molecular portrait of microsatellite instability across multiple cancers." Nat Commun **8**: 15180.

Cunningham, J. M., E. R. Christensen, D. J. Tester, C. Y. Kim, P. C. Roche, L. J. Burgart and S. N. Thibodeau (1998). "Hypermethylation of the hMLH1 promoter in colon cancer with microsatellite instability." Cancer Res **58**(15): 3455-3460.

Ellis, N. A., J. Groden, T. Z. Ye, J. Straughen, D. J. Lennon, S. Ciocci, M. Proytcheva and J. German (1995). "The Bloom's syndrome gene product is homologous to RecQ helicases." Cell **83**(4): 655-666.

Goswami, S. and P. Sharma (2017). "Genetic biomarker for cancer immunotherapy." Science **357**(6349): 358.

Goto, M., Y. Ishikawa, M. Sugimoto and Y. Furuichi (2013). "Werner syndrome: a changing pattern of clinical manifestations in Japan (1917~2008)." Biosci Trends **7**(1): 13-22.

Gray, M. D., J. C. Shen, A. S. Kamath-Loeb, A. Blank, B. L. Sopher, G. M. Martin, J. Oshima and L. A. Loeb (1997). "The Werner syndrome protein is a DNA helicase." Nat Genet **17**(1): 100-103.

Hampel, H., W. L. Frankel, E. Martin, M. Arnold, K. Khanduja, P. Kuebler, H. Nakagawa, K. Sotamaa, T. W. Prior, J. Westman, J. Panescu, D. Fix, J. Lockman, I. Comeras and A. de la Chapelle (2005). "Screening for the Lynch syndrome (hereditary nonpolyposis colorectal cancer)." N Engl J Med **352**(18): 1851-1860.

Herman, J. G., A. Umar, K. Polyak, J. R. Graff, N. Ahuja, J. P. Issa, S. Markowitz, J. K. Willson, S. R. Hamilton, K. W. Kinzler, M. F. Kane, R. D. Kolodner, B. Vogelstein, T. A. Kunkel and S. B. Baylin (1998). "Incidence and functional consequences of hMLH1 promoter hypermethylation in colorectal carcinoma." Proc Natl Acad Sci U S A **95**(12): 6870-6875.

Hickson, I. D. (2003). "RecQ helicases: caretakers of the genome." Nat Rev Cancer **3**(3): 169-178.

Huang, S., L. Lee, N. B. Hanson, C. Lenaerts, H. Hoehn, M. Poot, C. D. Rubin, D. F. Chen, C. C. Yang, H. Juch, T. Dorn, R. Spiegel, E. A. Oral, M. Abid, C. Battisti, E. Lucci-Cordisco, G. Neri, E. H. Steed, A. Kidd, W. Isley, D. Showalter, J. L. Vittone, A. Konstantinow, J. Ring, P. Meyer, S. L. Wenger, A. von Herbay, U. Wollina, M. Schuelke, C. R. Huizenga, D. F. Leistritz, G. M. Martin, I. S. Mian and J. Oshima (2006). "The spectrum of WRN mutations in Werner syndrome patients." Hum Mutat **27**(6): 558-567.

Huang, S., B. Li, M. D. Gray, J. Oshima, I. S. Mian and J. Campisi (1998). "The premature ageing syndrome protein, WRN, is a 3'-->5' exonuclease." Nat Genet **20**(2): 114-116.

Ionov, Y., M. A. Peinado, S. Malkhosyan, D. Shibata and M. Perucho (1993). "Ubiquitous somatic mutations in simple repeated sequences reveal a new mechanism for colonic carcinogenesis." Nature **363**(6429): 558-561.

Jiricny, J. (2006). "The multifaceted mismatch-repair system." Nat Rev Mol Cell Biol **7**(5): 335-346.

Kamath-Loeb, A. S., J. C. Shen, L. A. Loeb and M. Fry (1998). "Werner syndrome protein. II. Characterization of the integral 3' --> 5' DNA exonuclease." J Biol Chem **273**(51): 34145-34150.

Kaufman, B., R. Shapira-Frommer, R. K. Schmutzler, M. W. Audeh, M. Friedlander, J. Balmana, G. Mitchell, G. Fried, S. M. Stemmer, A. Hubert, O. Rosengarten, M. Steiner, N. Loman, K. Bowen, A. Fielding and S. M. Domchek (2015). "Olaparib monotherapy in patients with advanced cancer and a germline BRCA1/2 mutation." J Clin Oncol **33**(3): 244-250.

Kinzler, K. W. and B. Vogelstein (1997). "Cancer-susceptibility genes. Gatekeepers and caretakers." Nature **386**(6627): 761, 763.

Kitao, S., A. Shimamoto, M. Goto, R. W. Miller, W. A. Smithson, N. M. Lindor and Y. Furuichi (1999). "Mutations in RECQL4 cause a subset of cases of Rothmund-Thomson syndrome." Nat Genet **22**(1): 82-84.

Korch, C., M. A. Spillman, T. A. Jackson, B. M. Jacobsen, S. K. Murphy, B. A. Lessey, V. C. Jordan and A. P. Bradford (2012). "DNA profiling analysis of endometrial and ovarian cell lines reveals misidentification, redundancy and contamination." Gynecol Oncol **127**(1): 241-248.

Kuismanen, S. A., M. T. Holmberg, R. Salovaara, A. de la Chapelle and P. Peltomaki (2000). "Genetic and epigenetic modification of MLH1 accounts for a major share of microsatellite-unstable colorectal cancers." Am J Pathol **156**(5): 1773-1779.

Le, D. T., J. N. Durham, K. N. Smith, H. Wang, B. R. Bartlett, L. K. Aulakh, S. Lu, H. Kemberling, C. Wilt, B. S. Luber, F. Wong, N. S. Azad, A. A. Rucki, D. Laheru, R. Donehower, A. Zaheer, G. A. Fisher, T. S. Crocenzi, J. J. Lee, T. F. Greten, A. G. Duffy, K. K. Ciombor, A. D. Eyring, B. H. Lam, A. Joe, S. P. Kang, M. Holdhoff, L. Danilova, L. Cope, C. Meyer, S. Zhou, R. M. Goldberg, D. K. Armstrong, K. M. Bever, A. N. Fader, J. Taube, F. Housseau, D. Spetzler, N. Xiao, D. M. Pardoll, N. Papadopoulos, K. W. Kinzler, J. R. Eshleman, B. Vogelstein, R. A. Anders and L. A. Diaz, Jr. (2017). "Mismatch repair deficiency predicts response of solid tumors to PD-1 blockade." Science **357**(6349): 409-413.

Le, D. T., J. N. Uram, H. Wang, B. R. Bartlett, H. Kemberling, A. D. Eyring, A. D. Skora, B. S. Luber, N. S. Azad, D. Laheru, B. Biedrzycki, R. C. Donehower, A. Zaheer, G. A. Fisher, T. S. Crocenzi, J. J. Lee, S. M. Duffy, R. M. Goldberg, A. de la Chapelle, M. Koshiji, F. Bhaijee, T. Huebner, R. H. Hruban, L. D. Wood, N. Cuka, D. M. Pardoll, N. Papadopoulos, K. W. Kinzler, S. Zhou, T. C. Cornish, J. M. Taube, R. A. Anders, J. R. Eshleman, B. Vogelstein and L. A. Diaz, Jr. (2015). "PD-1 Blockade in Tumors with Mismatch-Repair Deficiency." N Engl J Med **372**(26): 2509-2520.

Lebel, M. and P. Leder (1998). "A deletion within the murine Werner syndrome helicase induces sensitivity to inhibitors of topoisomerase and loss of cellular proliferative capacity." Proc Natl Acad Sci U S A **95**(22): 13097-13102.

Lombard, D. B., C. Beard, B. Johnson, R. A. Marciniak, J. Dausman, R. Bronson, J. E. Buhlmann, R. Lipman, R. Curry, A. Sharpe, R. Jaenisch and L. Guarente (2000). "Mutations in the WRN gene in mice accelerate mortality in a p53-null background." Mol Cell Biol **20**(9): 3286-3291.

Lord, C. J. and A. Ashworth (2017). "PARP inhibitors: Synthetic lethality in the clinic." Science **355**(6330): 1152-1158.

Lynch, H. T. and A. J. Krush (1971). "Cancer family "G" revisited: 1895-1970." Cancer **27**(6): 1505-1511.

Mackenzie, K. J., P. Carroll, C. A. Martin, O. Murina, A. Fluteau, D. J. Simpson, N. Olova, H. Sutcliffe, J. K. Rainger, A. Leitch, R. T. Osborn, A. P. Wheeler, M. Nowotny, N. Gilbert, T. Chandra, M. A. M. Reijns and A. P. Jackson (2017). "cGAS surveillance of micronuclei links genome instability to innate immunity." Nature **548**(7668): 461-465.

Matsumoto, T., A. Shimamoto, M. Goto and Y. Furuichi (1997). "Impaired nuclear localization of defective DNA helicases in Werner's syndrome." Nat Genet **16**(4): 335-336.

McDonald, E. R., 3rd, A. de Weck, M. R. Schlabach, E. Billy, K. J. Mavrakis, G. R. Hoffman, D. Belur, D. Castelletti, E. Frias, K. Gampa, J. Golji, I. Kao, L. Li, P. Megel, T. A. Perkins, N. Ramadan, D. A. Ruddy, S. J. Silver, S. Sovath, M. Stump, O. Weber, R. Widmer, J. Yu, K. Yu, Y. Yue, D. Abramowski, E. Ackley, R. Barrett, J. Berger, J. L. Bernard, R. Billig, S. M. Brachmann, F. Buxton, R. Caothien, J. X. Caushi, F. S. Chung, M. Cortes-Cros, R. S. deBeaumont, C. Delaunay, A. Desplat, W. Duong, D. A. Dwoske, R. S. Eldridge, A. Farsidjani, F. Feng, J. Feng, D. Flemming, W. Forrester, G. G. Galli, Z. Gao, F. Gauter, V. Gibaja, K. Haas, M. Hattenberger, T. Hood, K. E. Hurov, Z. Jagani, M. Jenal, J. A. Johnson, M. D. Jones, A. Kapoor, J. Korn, J. Liu, Q. Liu, S. Liu, Y. Liu, A. T. Loo, K. J. Macchi, T. Martin, G. McAllister, A. Meyer, S. Molle, R. A. Pagliarini, T. Phadke, B. Repko, T. Schouwey, F. Shanahan, Q. Shen, C. Stamm, C. Stephan, V. M. Stucke, R. Tiedt, M. Varadarajan, K. Venkatesan, A. C. Vitari, M. Wallroth, J. Weiler, J. Zhang, C. Mickanin, V. E. Myer, J. A. Porter, A. Lai, H. Bitter, E. Lees, N. Keen, A. Kauffmann, F.

570 Stegmeier, F. Hofmann, T. Schmelzle and W. R. Sellers (2017). "Project DRIVE: A Compendium
571 of Cancer Dependencies and Synthetic Lethal Relationships Uncovered by Large-Scale, Deep
572 RNAi Screening." Cell **170**(3): 577-592 e510.

573 Mecklin, J. P. and H. J. Jarvinen (1991). "Tumor spectrum in cancer family syndrome (hereditary
574 nonpolyposis colorectal cancer)." Cancer **68**(5): 1109-1112.

575 Medico, E., M. Russo, G. Picco, C. Cancelliere, E. Valtorta, G. Corti, M. Buscarino, C. Isella, S.
576 Lamba, B. Martinoglio, S. Veronese, S. Siena, A. Sartore-Bianchi, M. Beccuti, M. Mottolese, M.
577 Linnebacher, F. Cordero, F. Di Nicolantonio and A. Bardelli (2015). "The molecular landscape of
578 colorectal cancer cell lines unveils clinically actionable kinase targets." Nat Commun **6**: 7002.

579 Nickoloff, J. A., D. Jones, S. H. Lee, E. A. Williamson and R. Hromas (2017). "Drugging the
580 Cancers Addicted to DNA Repair." J Natl Cancer Inst **109**(11).

581 O'Brien, V. and R. Brown (2006). "Signalling cell cycle arrest and cell death through the MMR
582 System." Carcinogenesis **27**(4): 682-692.

583 Overman, M. J., S. Lonardi, K. Y. M. Wong, H. J. Lenz, F. Gelsomino, M. Aglietta, M. A. Morse,
584 E. Van Cutsem, R. McDermott, A. Hill, M. B. Sawyer, A. Hendlisz, B. Neyns, M. Svrcek, R. A.
585 Moss, J. M. Ledeine, Z. A. Cao, S. Kamble, S. Kopetz and T. Andre (2018). "Durable Clinical
586 Benefit With Nivolumab Plus Ipilimumab in DNA Mismatch Repair-Deficient/Microsatellite
587 Instability-High Metastatic Colorectal Cancer." J Clin Oncol **36**(8): 773-779.

588 Peltomaki, P., R. A. Lothe, L. A. Aaltonen, L. Pylkkanen, M. Nystrom-Lahti, R. Seruca, L. David,
589 R. Holm, D. Ryberg, A. Haugen and et al. (1993). "Microsatellite instability is associated with
590 tumors that characterize the hereditary non-polyposis colorectal carcinoma syndrome." Cancer
591 Res **53**(24): 5853-5855.

592 Prince, P. R., M. J. Emond and R. J. Monnat, Jr. (2001). "Loss of Werner syndrome protein
593 function promotes aberrant mitotic recombination." Genes Dev **15**(8): 933-938.

594 Qi, Y. (2012). Random Forest for Bioinformatics. Ensemble Machine Learning: Methods and
595 Applications. C. Zhang and Y. Ma. Boston, MA, Springer US**:** 307-323.

596 Rosenthal, A. S., T. S. Dexheimer, G. Nguyen, O. Gileadi, A. Vindigni, A. Simeonov, A. Jadhav, I.
597 Hickson and D. J. Maloney (2010). Discovery of ML216, a Small Molecule Inhibitor of Bloom
598 (BLM) Helicase. Probe Reports from the NIH Molecular Libraries Program. Bethesda (MD).

599 Shen, J. C., M. D. Gray, J. Oshima, A. S. Kamath-Loeb, M. Fry and L. A. Loeb (1998). "Werner
600 syndrome protein. I. DNA helicase and dna exonuclease reside on the same polypeptide." J Biol
601 Chem **273**(51): 34139-34144.

602 Shi, J., E. Wang, J. P. Milazzo, Z. Wang, J. B. Kinney and C. R. Vakoc (2015). "Discovery of
603 cancer drug targets by CRISPR-Cas9 screening of protein domains." Nat Biotechnol **33**(6): 661-
604 667.

605 Siitonen, H. A., O. Kopra, H. Kaariainen, H. Haravuori, R. M. Winter, A. M. Saamanen, L.
606 Peltonen and M. Kestila (2003). "Molecular defect of RAPADILINO syndrome expands the
607 phenotype spectrum of RECQL diseases." Hum Mol Genet **12**(21): 2837-2844.

608 Streit, M., S. Gratzl, H. Stitz, A. Wernitznig, T. Zichner and C. Haslinger (2018). "Ordino: a visual
609 analysis tool for ranking and exploring genes, cell lines, and tissue samples." bioRxiv.

610 Van Maldergem, L., H. A. Siitonen, N. Jalkh, E. Chouery, M. De Roy, V. Delague, M. Muenke, E.
611 W. Jabs, J. Cai, L. L. Wang, S. E. Plon, C. Fourneau, M. Kestila, Y. Gillerot, A. Megarbane and
612 A. Verloes (2006). "Revisiting the craniosynostosis-radial ray hypoplasia association: Baller-
613 Gerold syndrome caused by mutations in the RECQL4 gene." J Med Genet **43**(2): 148-152.

614 Yu, C. E., J. Oshima, Y. H. Fu, E. M. Wijsman, F. Hisama, R. Alisch, S. Matthews, J. Nakura, T.
615 Miki, S. Ouais, G. M. Martin, J. Mulligan and G. D. Schellenberg (1996). "Positional cloning of
616 the Werner's syndrome gene." Science **272**(5259): 258-262.

617

Figure and Table Legends

Figure 1 – WRN is a selective dependency in MSI-H cancer cell models

A – WRN shRNA activity by RSA score in pooled shRNA depletion screens from Project DRIVE (McDonald, de Weck et al. 2017). Cell lines were binned according to tumor type.

B – MSS/MSI-H status and WRN RSA of CRC, endometrial and gastric cancer models from Project DRIVE.

Figure 2 – Loss of WRN selectively impairs viability of MSI-H CRC and endometrial cancer cell models

A – MSS and MSI-H CRC cell lines were transfected with the indicated siRNAs. Cell viability was determined 7 days after transfection and is shown relative to non-targeting control (NTC) siRNA. WRN siRNA knock-down efficacy was analyzed by immunoblotting. Protein lysates were prepared 72 h after transfection. GAPDH expression was used to monitor equal loading.

B – Crystal violet staining of MSS and MSI-H CRC lines treated as in panel A.

C – Cell viability analysis of MSS and MSI-H endometrial cell lines treated as in panel A.

Data information: In (A and C), data are presented as mean ± SD of three independent experiments.

Figure 3 – CRISPR/Cas9-mediated knock-out of WRN confirms the selective dependency of MSI-H CRC models on WRN

A – Schematic representation of CRISPR/Cas9 depletion assays. Cas9 expressing cells were transduced with a lentivirus encoding GFP and sgRNAs. The percentage of GFP-positive cells was determined over time by flow cytometry.

B – Cas9 expressing MSS or MSI-H CRC cells were transduced with a lentivirus encoding GFP and sgRNAs targeting multiple domains in WRN as indicated. The percentage of GFP-positive cells was determined 14 days post-transduction and normalized to the fraction of GFP-positive cells at the first measurement. Depletion ratios are shown relative to the positive control RPA3 (n=1 experimental replicate). Domains are annotated according to PFAM entry Q14191. RQC, RecQ helicase family DNA-binding domain; HRDC, Helicase and RNase D C-terminal, HTH, helix-turn-helix motif.

Figure 4 – WRN dependency in MSI-H CRC is linked to its helicase function

A – Schematic representation of WRN domain structure. Location of nuclease- and ATPase-inactivating mutations in siRNA-resistant WRN (WRNr) expression constructs is indicated.

B – MSI-H CRC HCT 116 cells were stably transduced with FLAG-tagged wild-type or mutant forms of WRNr and monoclonal lines with similar WRNr expression levels were isolated. For WRNr wild-type, two clones with high and low transgene expression were selected to cover the expression range of WRNr variants. Anti-FLAG immunofluorescence analysis was performed to monitor homogenous expression of WRNr. Expression of WRNr wild-type and mutant forms and endogenous protein levels were determined using immunoblotting with anti-FLAG and anti-WRN antibodies. GAPDH expression was used to monitor equal loading. Scale bar, 20 µM.

C – WRNr-expressing HCT 116 cells were transfected with the indicated siRNAs. Cell viability was determined 7 days after transfection and is shown relative to NTC siRNA.

Figure 5 – WRN loss-of-function in MSI-H CRC has detrimental effects on cell division

A – MSS and MSI-H CRC cell lines were transfected with the indicated siRNAs. Immunofluorescence analysis was performed 96 h after transfection to determine the fraction of cells with chromosomal bridges and micronuclei. Examples with enhanced brightness are shown as insets. LAP2B signal intensity was adjusted in a subset of samples for uniform representation. Scale bar, 10 µm.

B – Statistical analysis of chromosomal bridge phenotypes observed in siRNA knock-down studies shown in panel A.

C – Statistical analysis of micronuclei phenotypes observed in siRNA knock-down studies shown in panel A.

Data information: In (B and C), data are presented as mean ± SD of two or three independent experiments (n≥410 cells).

Figure 6 – Time-lapse analysis of mitosis in WRN-depleted MSS and MSI-H CRC models

Mitotic live cell imaging in WRN-depleted MSS and MSI-H CRC cell lines. Cells were transfected with WRN siRNA #1. Cells were stained with Hoechst dye and were analyzed 24 h post siRNA transfection. Exemplary lagging chromosomes (arrow) and a chromatin bridge (asterisk) are designated. Duration of time-lapse is indicated in minutes. Scale bar, 5 µM.

Figure 7 – Loss of WRN function in MSI-H CRC causes severe chromosomal defects

A – MSS and MSI-H CRC cell lines were transfected with the indicated siRNAs. Mitotic chromosome spreads were prepared 72 h after transfection and visualized by microscopy. Non-homologous radial formations are designated by arrows, breaks are labeled with asterisks.

B – Quantification of chromosomal defects. The status of chromosomal breaks of individual metaphase spreads was categorized into normal, 1-5 breaks or more than 5 breaks (n≥28 spreads of two independently analyzed slides). Non-homologous radial formation was counted as two breaks.

Figure 1 – figure supplement 1 – WRN dependency correlates with MMR gene mutation status and MLH1 expression

A – Receiver operating characteristic curve and variable importance plot for Random Forest model. Note: <gene>_st denotes the mutational status of respective gene whereas <gene> denotes the expression of the respective gene in the variable importance plot.

B – MLH1 mRNA TPM and WRN RSA of cancer models from Project DRIVE. Genes involved in MMR are indicated in red font.

Data information: Cell line mutation and expression data were derived from the Ordino database (Streit, Gratzl et al. 2018).

Figure 2 – figure supplement 1 – Non-transformed cells do not display WRN dependency

A – WRN siRNA knock-down efficacy in endometrial carcinoma cell models was analyzed by qRT-PCR. RNA lysates were prepared 72 h after transfection. WRN mRNA expression is normalized to 18S rRNA levels (n=1 experimental replicate).

B – Non-transformed hTERT RPE-1 and HCT 116 cells were transfected with the indicated siRNAs. Cell viability was determined 7 days after transfection and is shown relative to NTC siRNA. WRN siRNA knock-down efficacy was analyzed by immunoblotting. Protein lysates were prepared 72 h after transfection. GAPDH expression was used to monitor equal loading.

C – *TP53*-wild-type CRC cell lines SK-CO-1 and HCT 116 cells were transfected with the indicated siRNAs. Cell viability and WRN siRNA knock-down efficacy was analyzed as in panelB.

Data information: In (A), data are presented as mean ± SD of three independent experiments, in (B and C) data are presented as mean ± SD of two independent experiments.

Figure 3 – figure supplement 1 – CRISPR/Cas9-mediated knock-out of WRN confirms the selective dependency of MSI-H CRC models on WRN

Cas9-GFP expressing MSS or MSI-H CRC cells were transduced with a lentivirus encoding GFP and sgRNAs targeting multiple domains in WRN as indicated. The percentage of GFP-positive cells was determined 14 days post-transduction normalized to the fraction of GFP-positive cells at the first measurement. Depletion ratios are shown relative to the positive control the positive control RPA3 (n=1 experimental replicate). Domains are annotated according to PFAM entry Q14191. RQC, RecQ helicase family DNA-binding domain; HRDC, Helicase and RNase D C-terminal, HTH, helix-turn-helix motif.

Figure 4 – figure supplement 1 – WRN dependency in MSI-H CRC is linked to its helicase function

A – MSI-H CRC RKO cells were stably transduced with FLAG-tagged wild-type or mutant forms of WRNr. Anti-FLAG immunofluorescence analysis was performed to monitor homogenous expression of WRNr. Overexpression of WRNr wild-type and mutant forms compared to endogenous protein levels was determined using immunoblotting with anti-FLAG and anti-WRN antibodies. GAPDH expression was used to monitor equal loading. Scale bar, 20 µM.

B – WRNr-expressing RKO cells were transfected with the indicated siRNAs. Cell viability was determined 7 days after transfection and is shown relative to NTC siRNA.

Table 1 – MSS/MSI-H status analysis of CRC, endometrial and gastric carcinoma cell lines

MSS/MSI-H status was analyzed using fluorescent PCR-based analysis of the mononucleotide microsatellite markers NR-21, BAT-26, BAT-35, NR-24 and MONO-27. Main peak sizes for the mononucleotide microsatellite markers are shown for the MSS control cell line K562 and CRC, endometrial and gastric carcinoma cell lines. Cell models were classified as MSS (blue) or MSI-H (red) according to the indicated size range classification of MSS alleles.

738 **Table 2 – Overview of cell lines used in this study**

739 Cell lines used in this study are listed with tumor type of origin, MSI/MSS status, vendor source,
740 and STR confirmation status. Variable STR profiles are reported for ISHIKAWA cells, consistent
741 with MSI-H status (Korch, Spillman et al. 2012).

742

743 **Table 3 – Sequences of sgRNAs used for CRISPR depletion studies**

744 Sequences of sgRNAs used for targeting WRN are listed in N- to C-terminal order according to
745 the representation in Figure 3 and Expanded View Figure 3. Domains are annotated according
746 to PFAM entry Q14191. RQC, RecQ helicase family DNA-binding domain; HRDC, Helicase and
747 RNase D C-terminal, HTH, helix-turn-helix motif. Negative and positive control sgRNA
748 sequences are also listed.

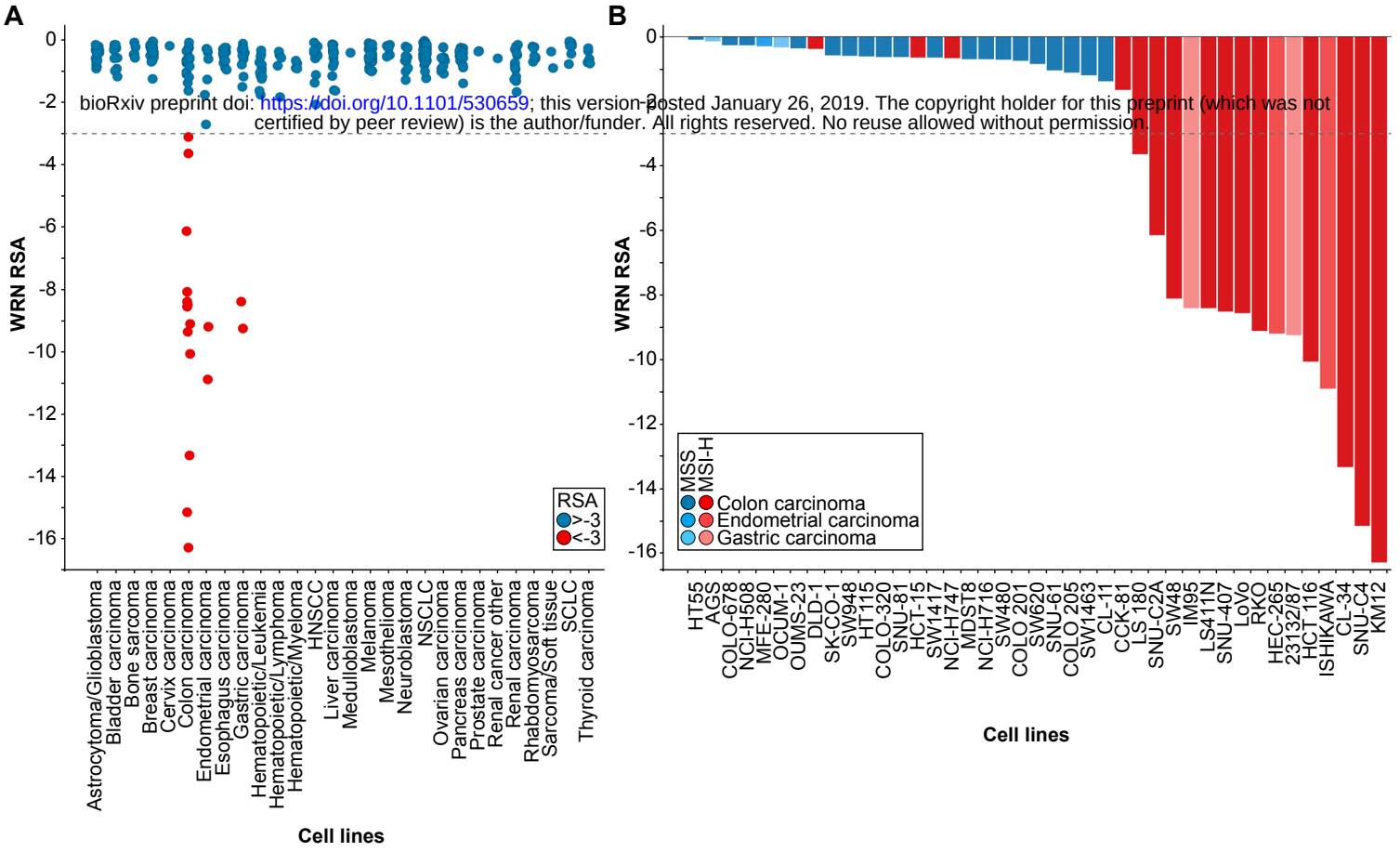

Lieb, Blaha-Ostermann *et al.* Figure 1

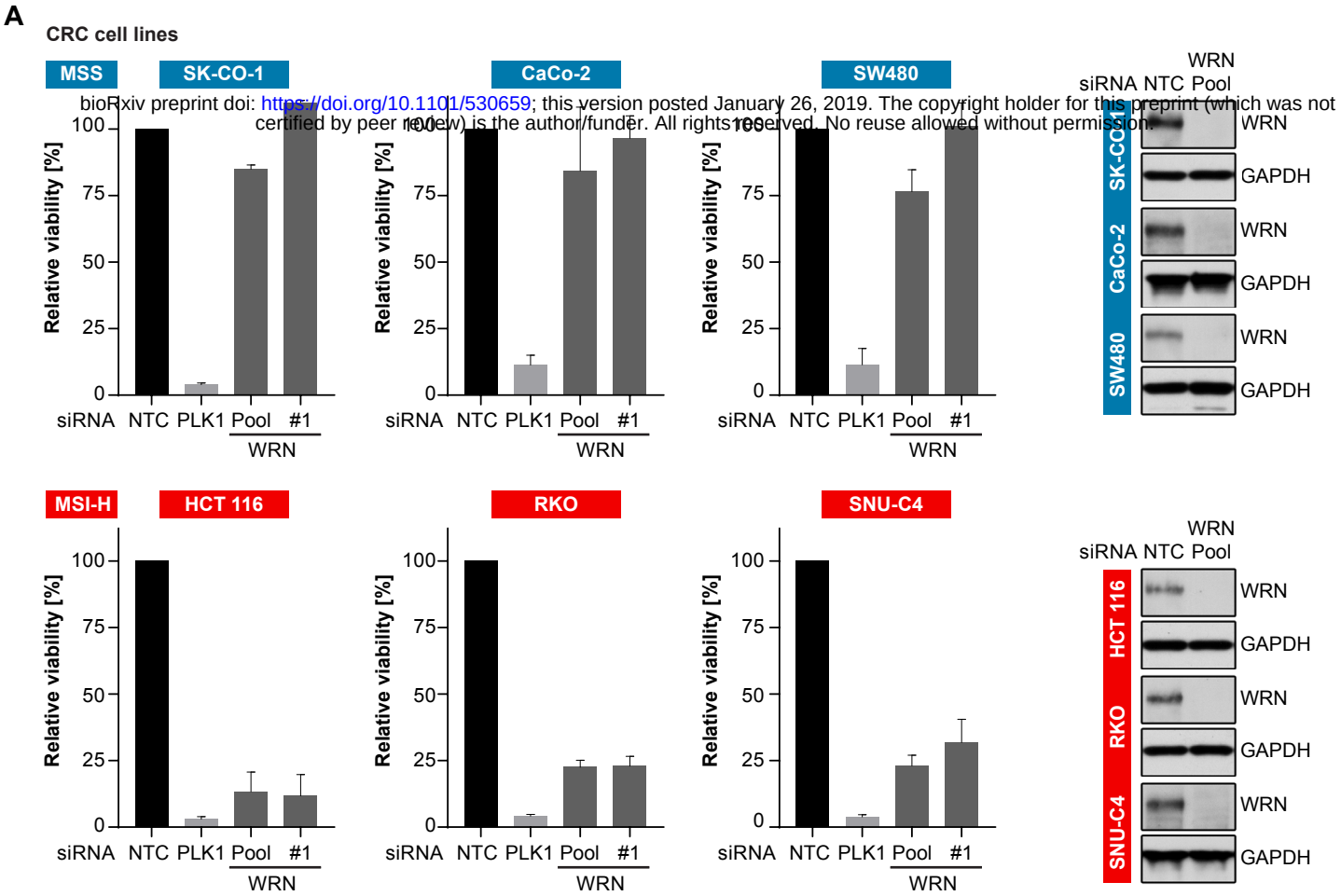

Lieb, Blaha-Ostermann *et al.* Figure 2

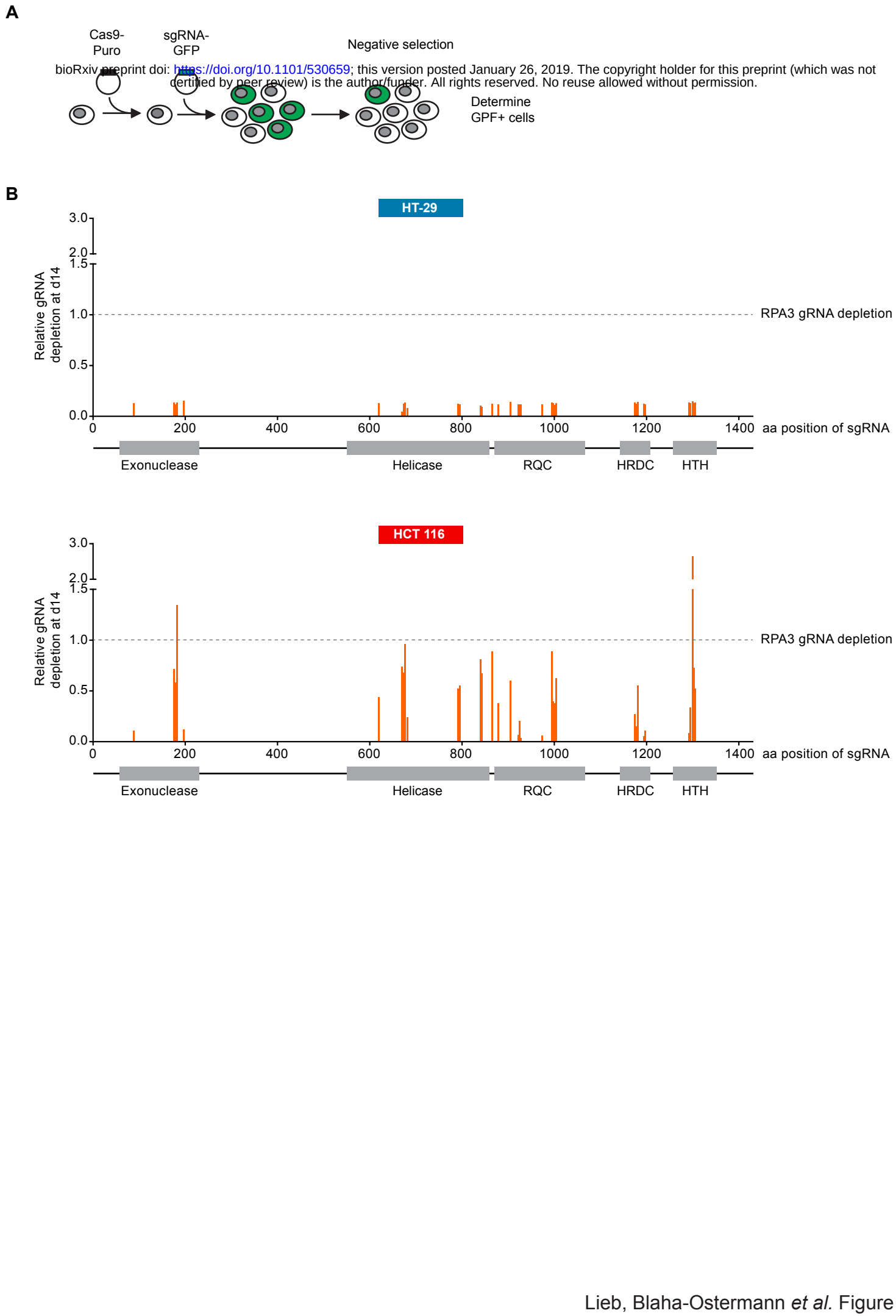

Lieb, Blaha-Ostermann *et al.* Figure 3

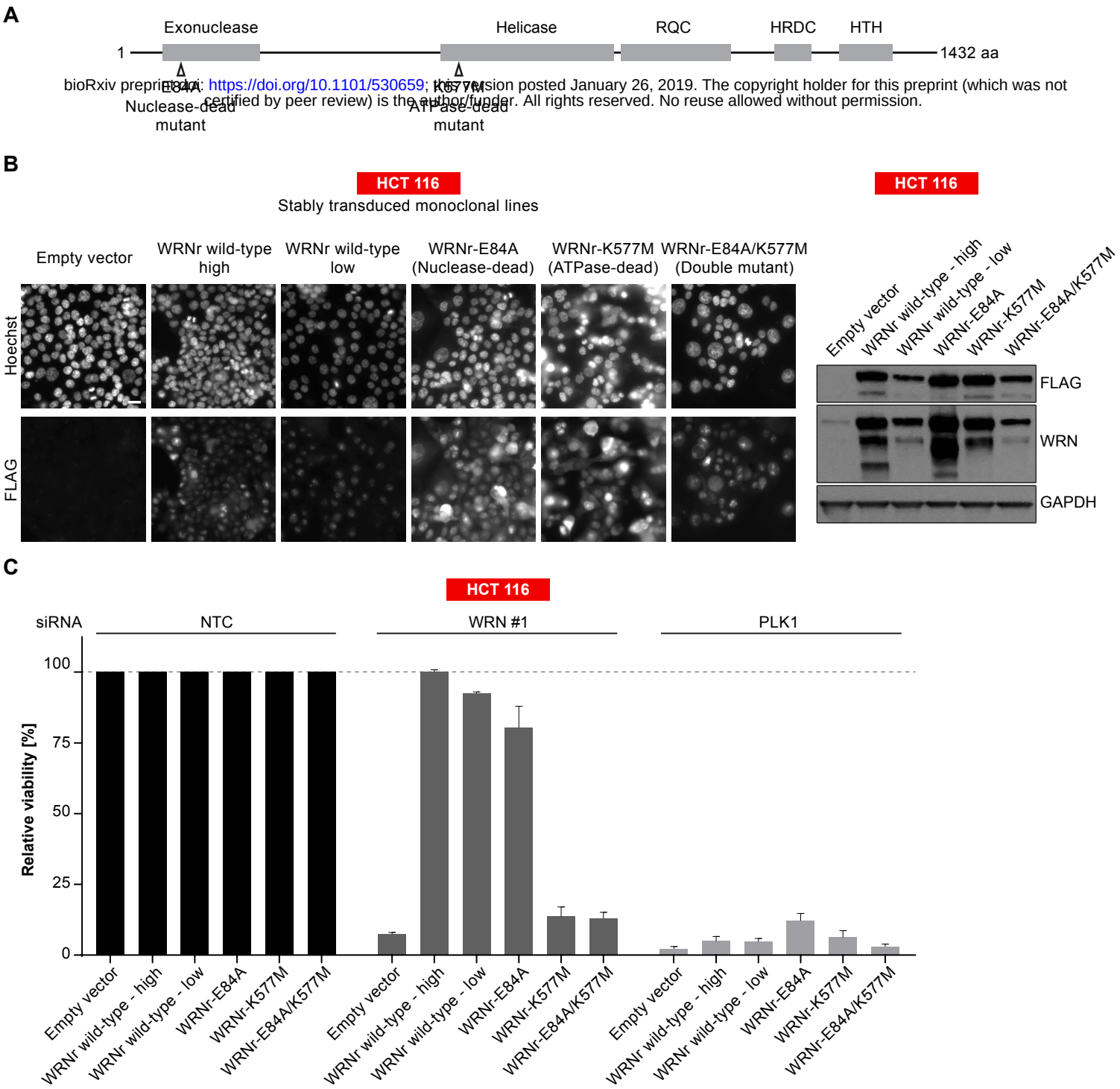

Lieb, Blaha-Ostermann *et al.* Figure 4

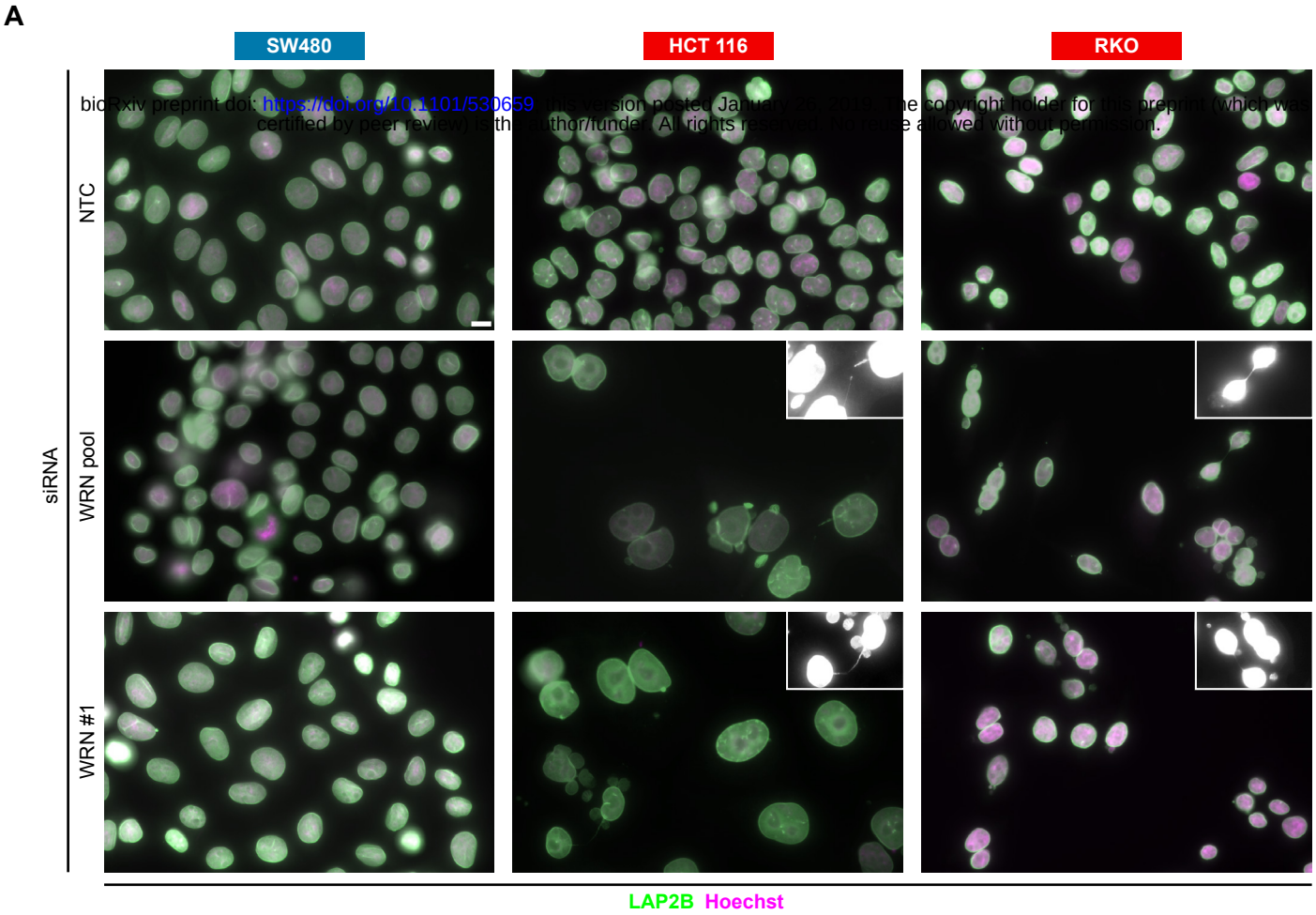

Lieb, Blaha-Ostermann *et al.* Figure 5

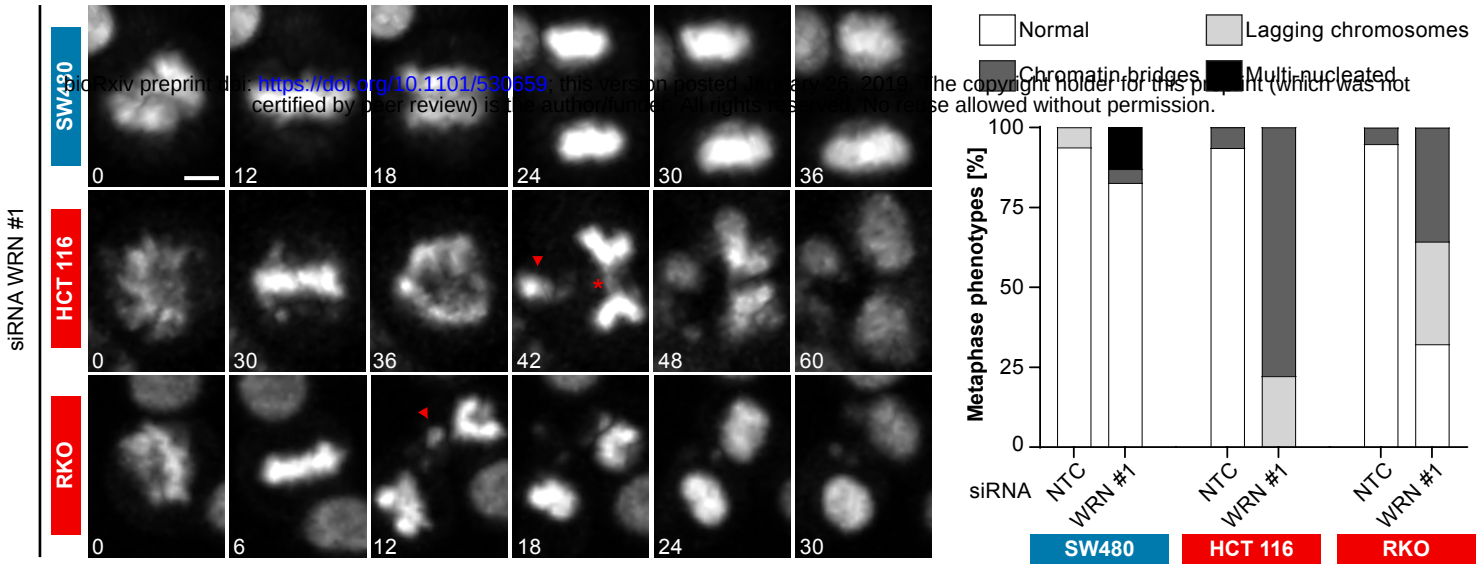

Lieb, Blaha-Ostermann *et al.* Figure 6

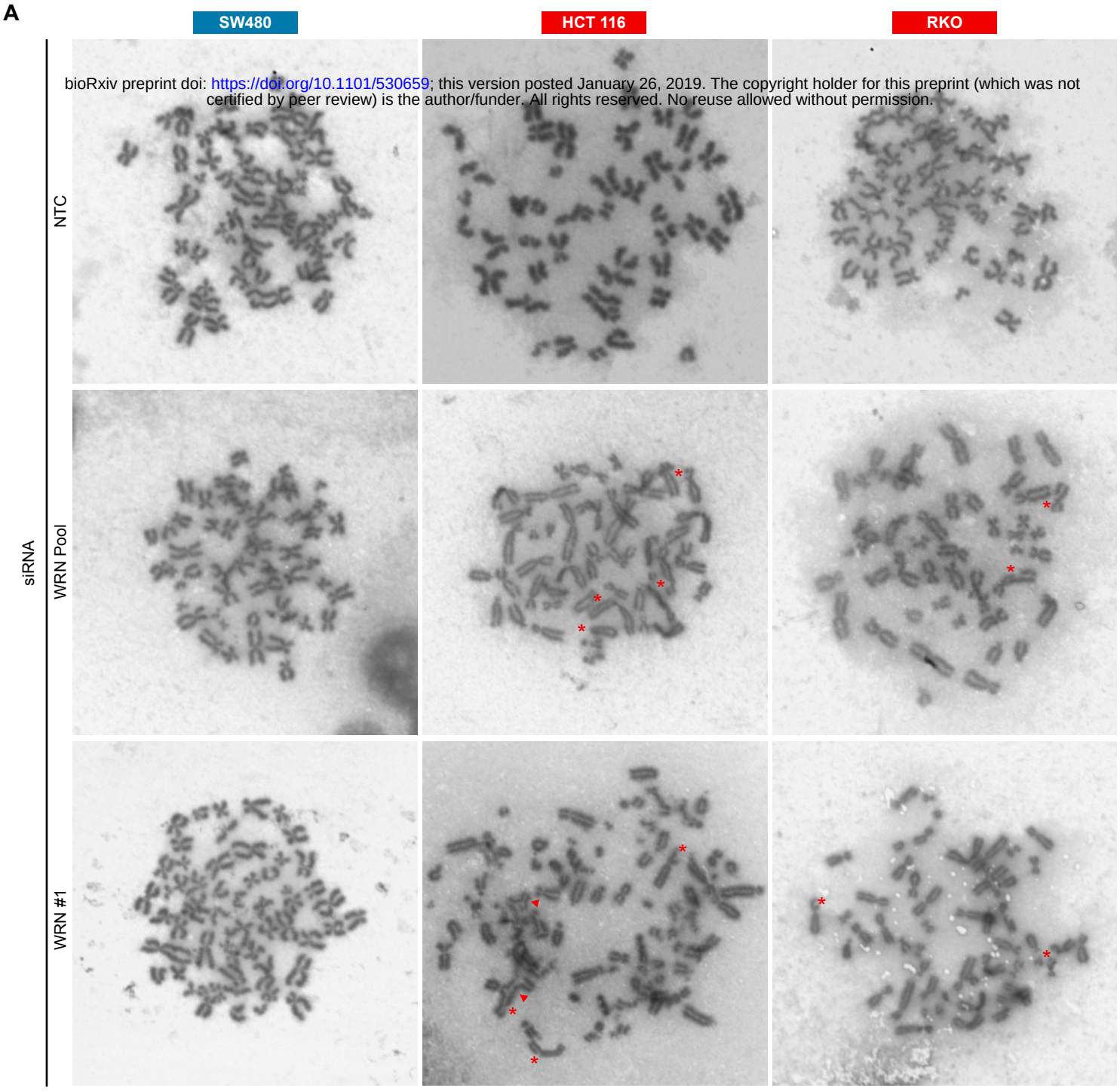

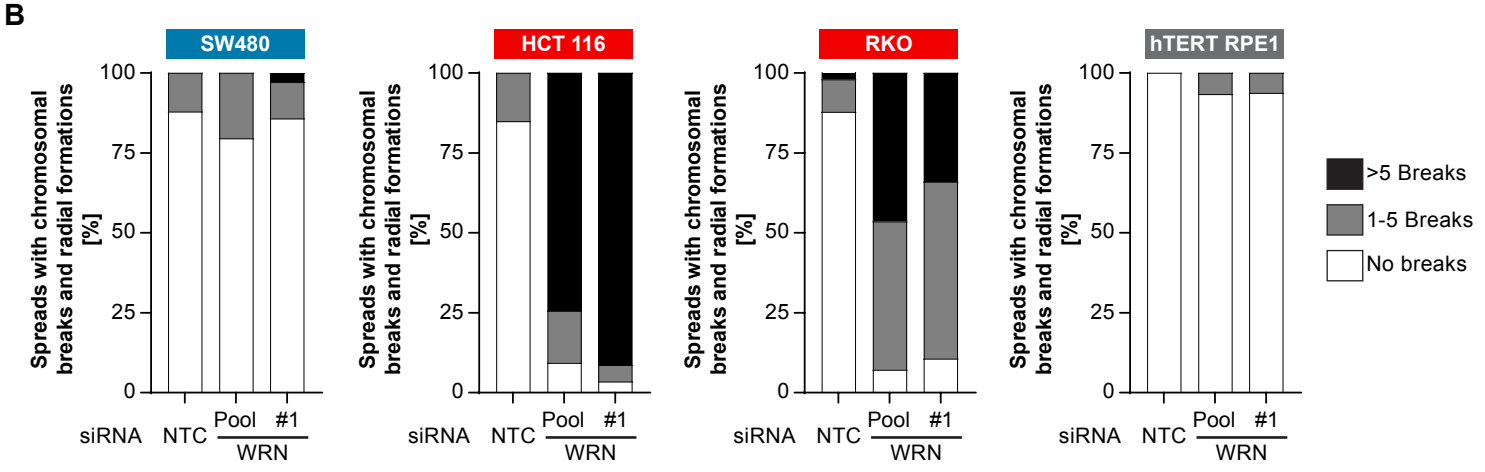

Lieb, Blaha-Ostermann *et al.* Figure 7

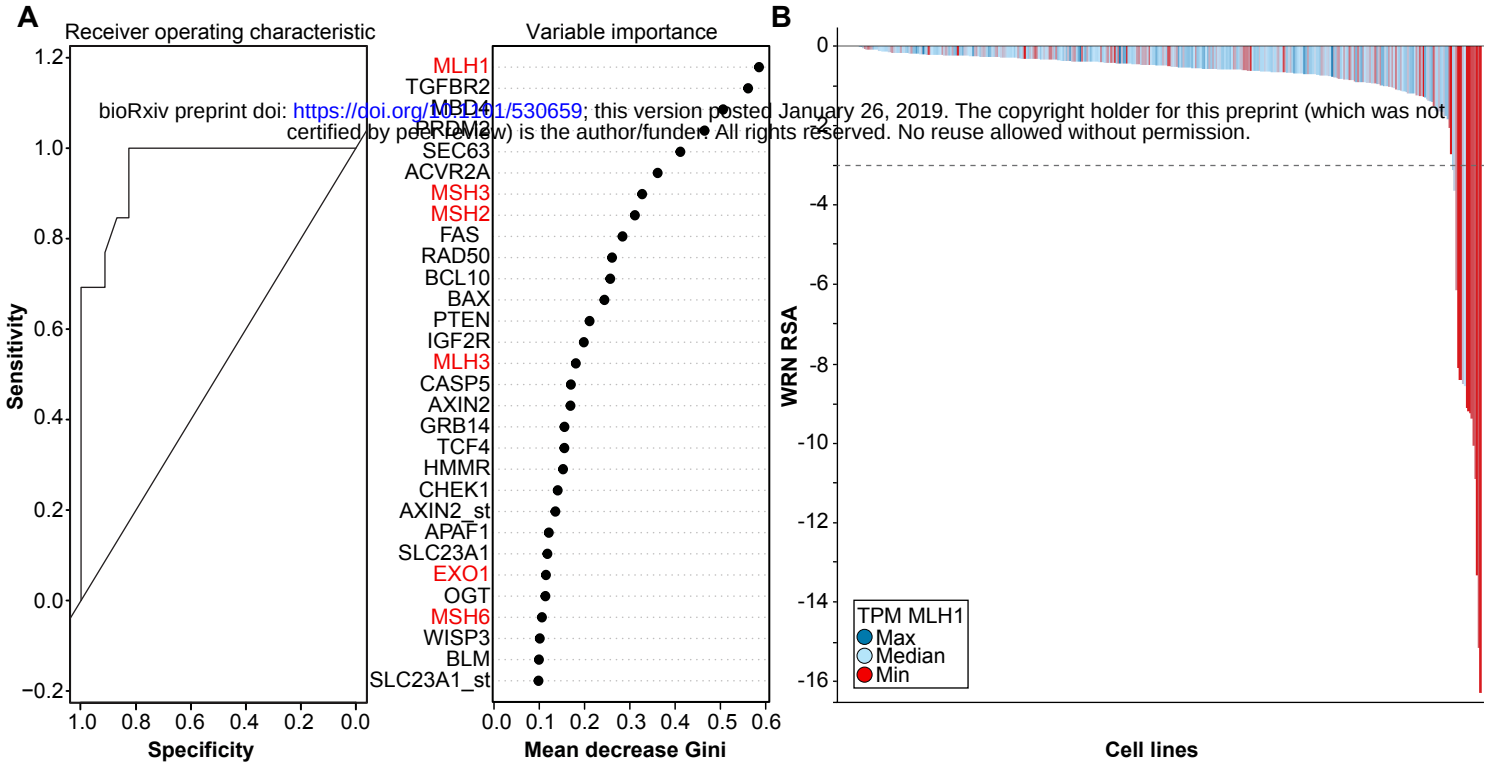

Lieb, Blaha-Ostermann *et al.* Figure 1 - figure supplement 1

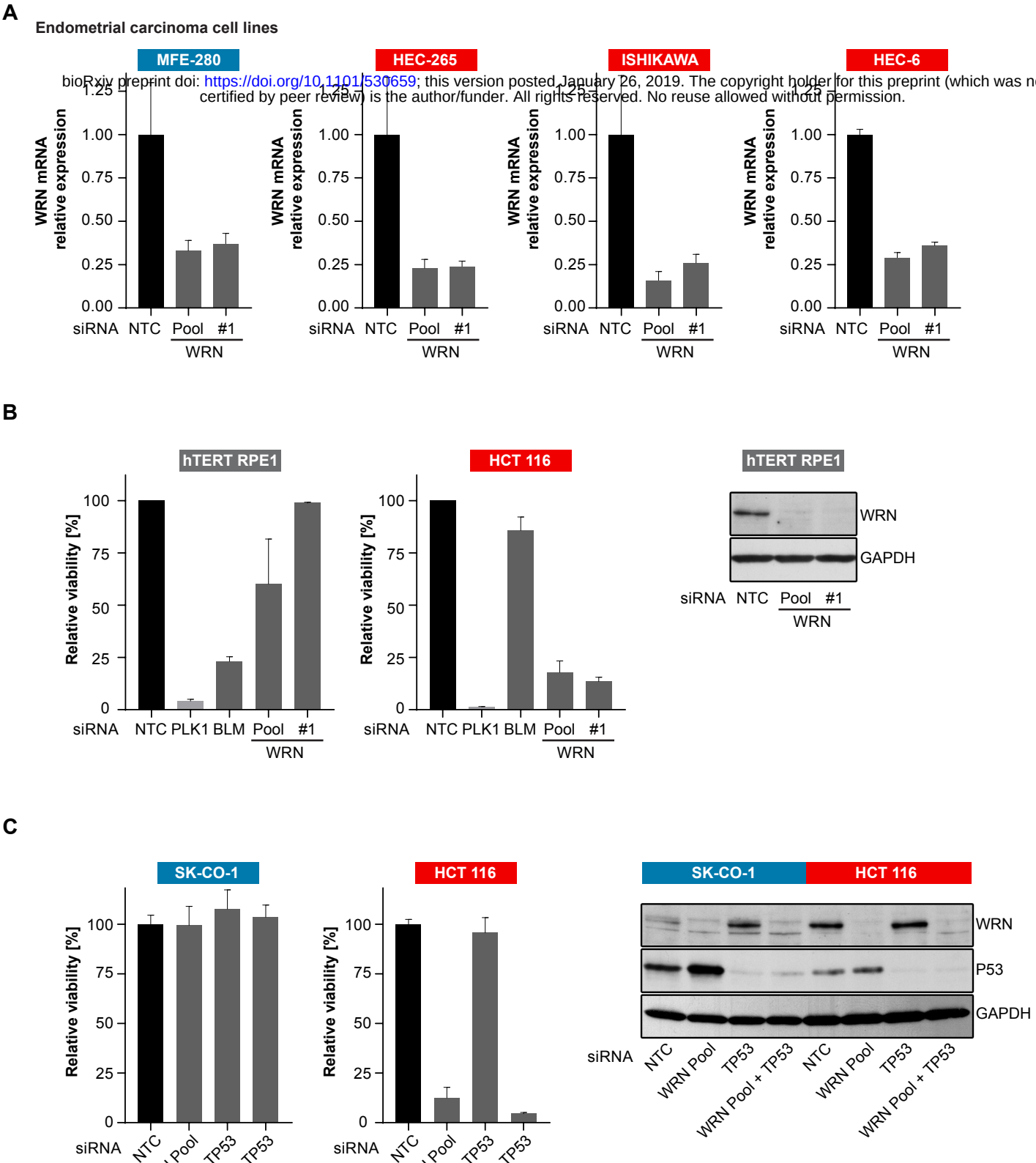

Lieb, Blaha-Ostermann *et al.* Figure 2 - figure supplement 1

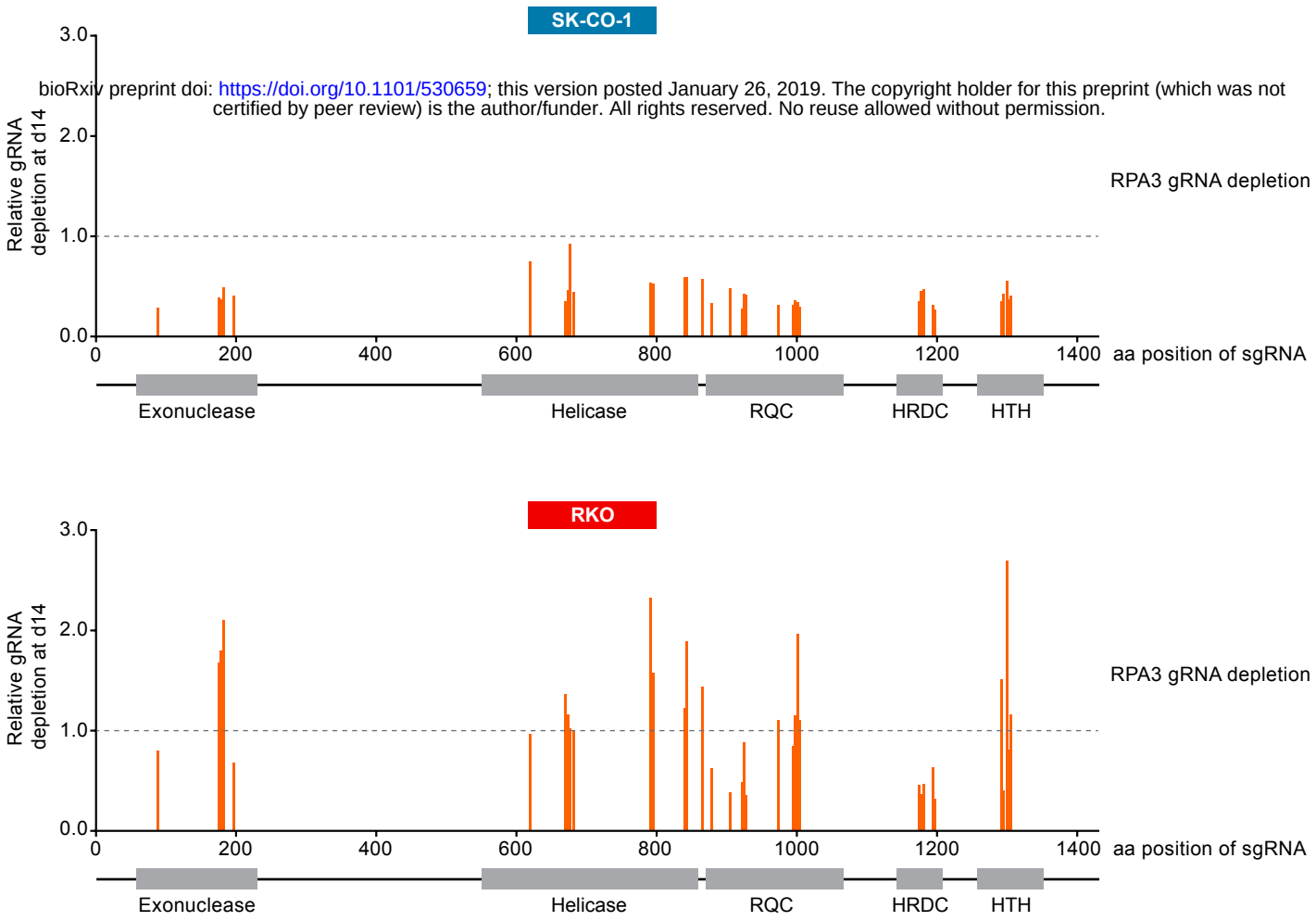

Lieb, Blaha-Ostermann *et al.* Figure 3 - figure supplement 1

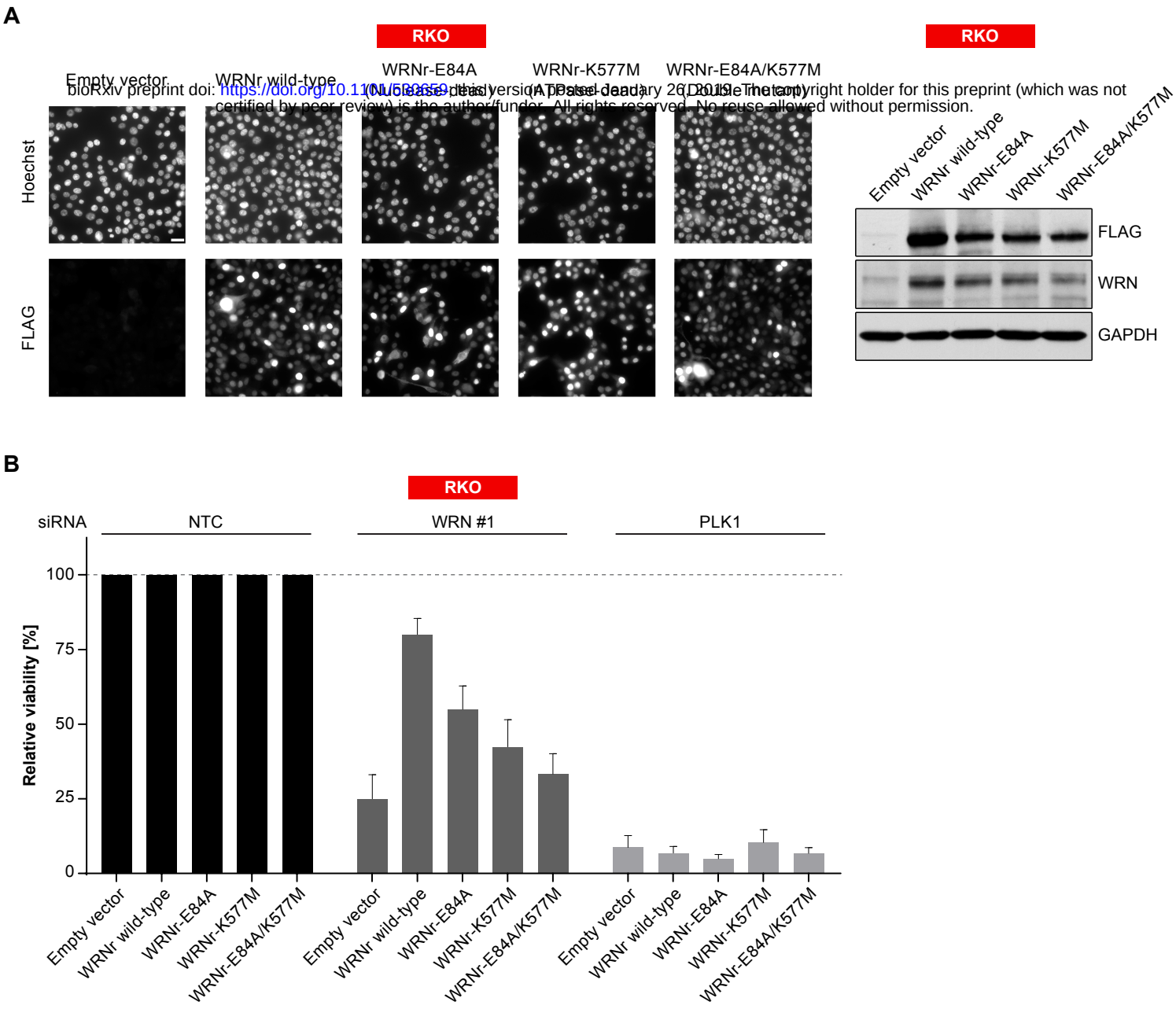

Table 1

		MSS control cell line	Normal retinal pigment epithelial cells
Marker	Size range (bp)	K562 (bp)	hTERT RPE-1 (bp)
NR-21	94-101	100.6	100.7
BAT-26	103-115	113.4	114.4
BAT-25	114-124	121.5	121.6
NR-24	130-133	130.1	130.0
MONO-27	142-154	149.9	149.0

	CRC cell lines					
Marker	SK-CO-1 (bp)	SW480 (bp)	CaCo-2 (bp)	HCT 116 (bp)	RKO (bp)	SNU-C4 (bp)
NR-21	100.6	99.6	99.7	92.3	87.0	90.3
BAT-26	114.4	113.4	113.5	101.9	102.7	101.8
BAT-25	121.5	120.5	121.8	115.2	112.1	114.2
NR-24	130.1	130.1	131.1	120.9	124.0	120.8
MONO-27	148.9	149.9	149.1	140.7	137.6	138.7

	Endometrial carcinoma cell lines			
Marker	MFE-280 (bp)	HEC-265 (bp)	ISHIKAWA (bp)	HEC-6 (bp)
NR-21	99.6	91.3	88.1	89.1
BAT-26	113.4	102.0	100.9	100.8
BAT-25	122.6	117.4	113.1	112.0
NR-24	131.1	123.9	123.0	123.0
MONO-27	148.9	143.8	140.7	141.7

	Gastric carcinoma cell lines			
Marker	AGS (bp)	OCUM-1 (bp)	23132.87 (bp)	IM95 (bp)
NR-21	98.6	99.6	89.2	94.4
BAT-26	113.4	113.4	101.9	101.9
BAT-25	121.5	121.6	114.2	114.2
NR-24	131.2	131.1	123.0	119.8
MONO-27	149.9	150.0	143.7	140.7

Table 2

Cell line	Tumor type	MSI/MSS status	Reference for MSI/MSS status
CaCo-2	CRC	MSS	Medico et al. (2015) Nat Commun 6: 7002, this study
HCT 116	CRC	MSI-H	Medico et al. (2015) Nat Commun 6: 7002, this study
HCT 116 _CRISPR-Cas9-Puro	CRC	MSI-H	Medico et al. (2015) Nat Commun 6: 7002, this study
HEC-265	Endometrial carcinoma	MSI-H	This study
HEC-6	Endometrial carcinoma	MSI-H	This study
HT-29_CRISPR-Cas9-Blasti	CRC	MSS	Medico et al. (2015) Nat Commun 6: 7002 (parental line)
hTERT RPE-1	Normal retinal pigment epithelial cells	MSS	This study
ISHIKAWA	Endometrial carcinoma	MSI-H	This study
LS1034	CRC	MSS	Medico et al. (2015) Nat Commun 6: 7002
MFE-280	Endometrial carcinoma	MSS	This study
RKO	CRC	MSI-H	Medico et al. (2015) Nat Commun 6: 7002, this study
RKO Cas9-puro	CRC	MSI-H	Medico et al. (2015) Nat Commun 6: 7002, this study (parental line)
SK-CO-1	CRC	MSS	Medico et al. (2015) Nat Commun 6: 7002, this study
SK-CO-1 Cas9-puro	CRC	MSS	Medico et al. (2015) Nat Commun 6: 7002, this study
SNU-C4	CRC	MSI-H	Medico et al. (2015) Nat Commun 6: 7002, this study
SW480	CRC	MSS	Medico et al. (2015) Nat Commun 6: 7002, this study

Cell line	Source	STR confirmed
CaCo-2	ATCC	Yes
HCT 116	ATCC	Yes
HCT 116 _CRISPR-Cas9-Puro	This study	Yes
HEC-265	JCRB1142	Yes
HEC-6	JCRB 1118	Yes
HT-29_CRISPR-Cas9-Blasti	This study	Ongoing
hTERT RPE-1	ATCC	Ongoing
ISHIKAWA	ECACC	No*
LS1034	ATCC	Yes
MFE-280	DSMZ	Near full
RKO	ATCC	Yes
RKO Cas9-puro	ATCC	Near full
SK-CO-1	ATCC	Yes
SK-CO-1 Cas9-puro	ATCC	Yes
SNU-C4	KCLRF	Yes
SW480	ATCC	Near full

* variable STR profiles reported consistent with MSI-H status (Korch et al. (2012) Gynecol Oncol 27(1):241-8)

Table 3

WRN domain targeting sgRNAs (N- to C-terminal order)	
Targeted domain	**sgRNA sequence**
Exonuclease	AGTCTATCCGCTGTAGCAAT
	GACCTGGAGCCTTAACAGTC
	AACCAGACTGTTAAGGCTCC
	AGTCTGGTTAAACACCTCTT
	GGCCACCATTATACAATAGA
Helicase	GCTCACTGTATTTCTGAGTG
	AGGCTCACTGTATTTCTGAG
	CTCACTGTATTTCTGAGTGG
	ATGATTTTAGGGATTCATTC
	TTTCTGACTGTGCTGATCCA
	CATTCATTACGGTGCTCCTA
	TTACGGTGCTCCTAAGGACA
	TGCTAAAACTCATGCCCGCA
	GCCCGCATGGTATGTTCCAC
	AAGTTCTTGTCACGTCCTCT
	CATTACGTATCTCAGTAAGA
	AGTTCCCATAATTCCCAAGG
	AAAGCCTCCTTGGGAATTAT
	ACAAGTACAAAAAGCCTCCT
	ATCTTCATTCTAGCAGATGT
RQC	GTCTTGCCGATCAATATCGC
	ACTGTGCCTGCGATATTGAT
	GACATCTTAGGCGAAAAATT
	AGGCACAGTTTATTTGGCAC
	TATCGCAGGCACAGTTTATT
HRDC	CTACGGTTGAAAACGTAAAA
	TTTACGTTTTCAACCGTAGT
	GTTTGTTGCCAGAATAGCTG
	TCTGGCAACAAACAAGATAC
	TTTGTTGCCAGAATAGCTGG
HTH	CCCCTTGATTTGGAGCGAGC
	TTATCCCAAGCGGTGAAAGC
	GGCAGCCAGCTTTCACCGCT
	GGCCTGCTCGCTCCAAATCA
	CTGCTCGCTCCAAATCAAGG
Control sgRNAs	**sgRNA sequence**
Neg#1	GGCAGTCGTTCGGTTGATAT
Neg#2	GATACACGAAGCATCACTAG
RPA3	GATGAATTGAGCTAGCATGC
PCNA	GGACTCGTCCCACGTCTCTT
POLR2A	GTACAATGCAGACTTTGACG